Resonant Brillouin scattering in CdS. II. Theory

M. Matsushita,* J. Wicksted,† and H. Z. Cummins
Physics Department, City College of the City University of New York, New York, New York 10031
(Received 3 June 1983)

Numerical calculations are presented for the observable external scattering cross sections of resonant Brillouin scattering. The A exciton in semiconducting CdS is taken as a concrete example with both the longitudinal-acoustic-phonon deformation potential and the transverse-acoustic-phonon piezoelectric potential scattering considered. Use is made of the factorization approximation for the external scattering cross section, and the internal cross section is formulated in detail quantum mechanically. Important factors contained in the scattering efficiency, exciton-polariton dispersion curves, scattered frequency, transmissivities (both from vacuum to medium and vice versa) with various additional boundary conditions, group and energy velocities, and exciton strength functions, are calculated separately, and are then combined to find the internal and the observable external scattering cross sections. While the internal cross section shows a monotonic increase as a function of incident frequency ω_I, with strong growth near the transverse exciton frequency ω_0, the curves describing the external cross sections are found to have characteristic structures around ω_0 and the longitudinal exciton frequency ω_L which depend strongly on the choice of additional boundary conditions. They are also shown to exhibit a drastic profile change when the exciton damping constant Γ approaches a threshold value Γ_c. Polariton effects are expected only for $\Gamma < \Gamma_c$, and the usual exciton "resonance" effects which are qualitatively different from those of the polariton are shown to occur for $\Gamma \gtrsim \Gamma_c$. The suitability of resonant Brillouin scattering for experimentally determining the proper additional boundary condition as well as values of the parameters of the exciton and exciton-polariton is discussed.

I. INTRODUCTION

The theory of resonant Brillouin scattering (RBS) in semiconducting crystals mediated by exciton polaritons[1–3] was first investigated by Brenig, Zeyher, and Birman (BZB) in 1972.[4] Their results indicated that RBS would provide a powerful technique for exploring the properties of exciton polaritons as well as for elucidating the additional boundary condition (ABC) problem of spatially dispersive dielectric media.[5]

BZB's analysis can be conveniently separated into two parts. First, there is a purely kinematic part which relates the Brillouin shifts to the exciton-polariton dispersion curves as shown schematically in Fig. 1. The exciton-polariton dispersion curves represent excitations moving into the crystal on the right, and moving back towards the crystal surface on the left. Thus for the usual backscattering geometry an incident polariton at ω_I is backscattered with the creation (Stokes) or annihilation (anti-Stokes) of an acoustic phonon. The straight lines joining incident and scattered polaritons are drawn with a slope equal to the sound velocity c_s of the acoustic mode, which automatically satisfies the requirements of conservation of energy and crystal momentum. For ω_I well below the transverse exciton frequency ω_0, there are two Brillouin components and the Brillouin shifts $|\omega_s - \omega_I|$ increase linearly with increasing ω_I. For ω_I above the longitudinal exciton frequency ω_L, there are two polariton modes for each ω_I, each of which can scatter to either the inner branch (1′) or outer branch (2′), giving rise to a Brillouin octet in place of the original Brillouin doublet as illustrated in Fig. 2. This part of BZB's analysis is independent of the details of both the scattering theory and the ABC's, and have been universally applied in the analysis of RBS

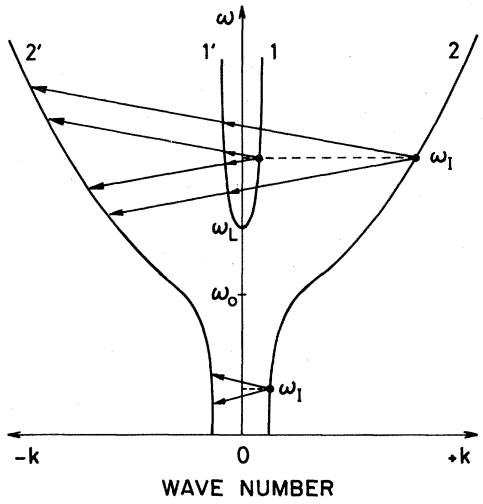

FIG. 1. Schematic representation of the exciton-polariton dispersion curve and the kinematics of backward Brillouin scattering. Dots indicate the initial polariton states. The arrows illustrate Stokes (downward) and anti-Stokes (upward) scatterings with incident frequency ω_I, and the inclination is the sound velocity involved in the scattering. Note that for ω_I well below ω_L there are the usual two scattering channels, while additional scattering channels appear for $\omega_I \gtrsim \omega_L$.

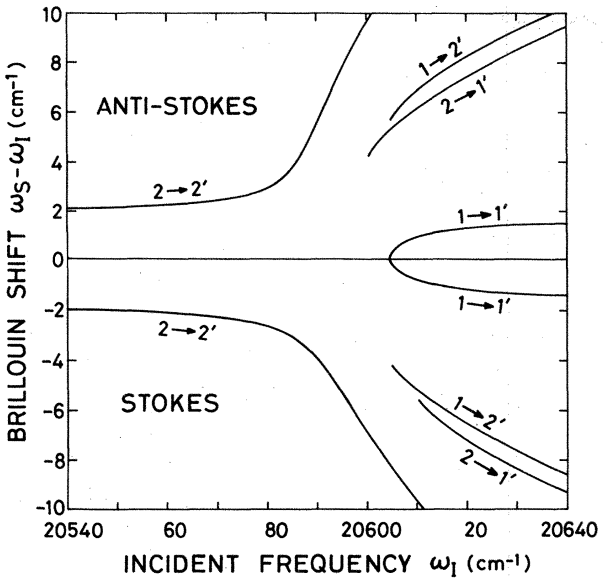

FIG. 2. Numerically calculated Stokes and anti-Stokes Brillouin shifts of the LA phonon as a function of incident laser frequency ω_I. The label $(i\rightarrow j')$ on each curve denotes the scattering channel from mode-i initial to mode-j final polaritons. The parameter values used are the same as those given in Fig. 4 with $\Gamma=1.0$ cm^{-1} and $c_{s\mathrm{LA}}=4.25\times10^5$ cm/sec.

experiments.

The second part of BZB's analysis concerns the scattering efficiencies or cross sections, and is far more complicated. The conventional method for relating observable (external) scattering cross sections to theoretical (internal) cross sections makes use of a factorization procedure in which photons of frequency ω_I incident at the crystal surface are converted to internal polaritons by a transmissivity factor $T(\omega_I)$, and scattered polaritons ω_s reaching the boundary are again converted to external photons via another transmissivity $T'(\omega_s)$. The transmission functions T and T' contain all the effects of the boundary conditions (for a discussion of the factorization procedure see Ref. 8). BZB avoided the factorization procedure by constructing wave fields with eigenmodes which are asymptotically free-photon-like far in the vacuum, and asymptotically polaritonlike far inside the crystal. A scattering event then scatters a quantum from one wave-field eigenmode to another, and observable cross sections and line shapes follow directly from first-order perturbative scattering theory without requiring the joining of internal and external modes via transmission factors (see Ref. 8).

BZB computed total scattering efficiencies for LA Brillouin scattering using three different ABC's. In their calculations the exciton damping parameter Γ was taken as 10 cm^{-1}, which is much too large since experimental evidence indicates that $\Gamma<1$ cm^{-1}. Several years later Yu[6] pointed out that BZB's value of $\Gamma=10$ cm^{-1} was so large that polariton effects would be suppressed (see Sec. IV for further discussion of this point). Yu computed the scattering efficiency for LA(2-2') scattering using two ABC's and three Γ values (1, 4, and 10 cm^{-1}), and showed that for $\Gamma=10$ cm^{-1} his result, obtained by a factorization procedure, closely resembled BZB's.

Since BZB's paper, no additional calculations of Brillouin cross sections have appeared based on their wave-field eigenmode method. Instead, various versions of the factorization procedure have been employed. This is primarily because BZB's method is not straightforward to implement, whereas the factorization procedure is ideally suited for computer analysis. The problem of equivalence of the two methods has never been fully resolved.[7] Zeyher, Ting, and Birman have shown that the two approaches are not generally equivalent in that when spatial dispersion effects are included, the cross section does not factorize into the product of transmission factors and an internal cross section.[8] However, the quantitative differences remain largely unevaluated.

In this paper we present a detailed derivation of the factorization procedure which is explicitly organized to produce numerical predictions for comparison with our experimental data in the preceding paper (hereafter designated as I). There have been three previous attempts to calculate RBS cross sections.[4,6,9] BZB (Ref. 4) and Yu[6] considered polaritons to be in a semi-infinite medium but phonons to be in an infinite one, i.e., they took into account the boundary conditions only for polaritons, while Tilley[9] regarded both polaritons and phonons as being in a semi-infinite medium, although he did not calculate the cross sections numerically. All these authors treated the polariton scattering process classically. In this paper, we will reformulate the RBS cross section, regarding both polaritons and phonons as being in a semi-infinite medium so as to be able to incorporate their boundary conditions into the cross section if necessary, as Tilley did. Moreover, we treat the polariton scattering completely quantum mechanically.[10–12] In this formulation the exciton-polariton scattering by longitudinal- or transverse-acoustic phonons (abbreviated as LA and TA, respectively) is assumed to take place via interaction of phonons with the exciton part of the polaritons.

We start by discussing briefly in Sec. II what is occurring in the RBS experiment and what we need to calculate. In Sec. III we formulate the internal scattering cross section of exciton polaritons quantum mechanically, based on the polariton-phonon-interaction Hamiltonian derived in Appendix A. Our approach is based on that of Burstein *et al.*[11] but differs somewhat from their approach since we take the damping of polaritons inside the medium into consideration explicitly. After making some plausible approximations we obtain results similar to BZB's. In Sec. IV we present the results of numerical calculations of the elements of the RBS cross section, i.e., exciton-polariton dispersion curves with various values of the exciton damping constant Γ, transmissivities of light both from vacuum to medium and from medium to vacuum with various ABC's, polariton group and energy velocities, and the exciton-strength function of polaritons. Finally, we combine these results to obtain the internal and external (observable) scattering cross sections. We point out the importance of the threshold value of the exciton damping constant, Γ_c (the derivation is given in Appendix B), which is responsible for the drastic profile change of the scattering efficiency curves as well as the dispersion curves with increasing Γ. The results are sum-

marized and discussed in Sec. V, confirming that Γ_c provides the appropriate criterion for the observation of polariton effects in RBS experiments.

II. RBS

Inherently, RBS must be studied in the vicinity of the resonant frequency ω_0 of the excitons under consideration, where damping of the polaritions is enhanced. The medium then becomes effectively opaque. Therefore, the backward scattering geometry is obligatory. From this point on we will assume this geometry unless otherwise stated. In RBS, incident polaritons inside a medium are produced by laser light from outside, and scattered polaritons are measured outside as photons. We must take into account, therefore, the transmissivities of incident and scattered photons, and the difference between the internal and external solid angle of the scattered photons. In RBS [or resonant Raman scattering (RRS)] these factors are very important, since as we will show later their values vary drastically with incident laser frequency ω_I near ω_0.

We begin by analyzing the scattering geometry illustrated in Fig. 3. $I_I^{\rm ext}(\omega_I)$ is the (time averaged) incident photon intensity in vacuum and $I_{Ii}^{\rm int}(\omega_I)$ the incident mode-i ($i=1$ or 2) polariton intensity (energy flow). $I_{Sj}^{\rm int}(\omega_S)$ and $I_{Sj}^{\rm ext}(\omega_S)$ are, respectively, the scattered mode-j ($j=1$ or 2) polariton intensity and the associated photon intensity.

The internal differential scattering cross section for polaritons is defined as the energy removed from the incident polariton mode i per unit time by events which produce scattering to polariton mode j per unit solid angle per unit scattered frequency interval, divided by the incident power flow:

$$\frac{\partial^2\sigma_{ij}^{\rm int}}{\partial\Omega^{\rm int}\partial\omega_s}=\frac{\omega_I}{\omega_s}\frac{R^2 I_{s_j}^{\rm int}(\omega_s)}{I_{I_i}^{\rm int}}\ , \tag{2.1}$$

where R is the distance from the scattering volume to the point of observation. The factor ω_I/ω_s accounts for the fact that each quantum $\hbar\omega_I$ removed from the incident beam generates a scattered quantum $\hbar\omega_s$, the difference in energy being transferred to (or removed from) the crystal.[13] The external differential scattering cross section per unit solid angle and frequency is then given via the factorization procedure by

$$\frac{\partial^2\sigma_{ij}^{\rm ext}}{\partial\Omega_j^{\rm ext}\partial\omega_S}=\frac{T_i(\omega_I)T_j'(\omega_S)}{n_j^2(\omega_S)}\frac{\partial^2\sigma_{ij}^{\rm int}}{\partial\Omega_j^{\rm int}\partial\omega_S}\ , \tag{2.2}$$

where $T_i=I_{Ii}^{\rm int}/I_I^{\rm ext}$ and $T_j'=I_{Sj}^{\rm ext}/I_{Sj}^{\rm int}$ are transmissivities from vacuum to medium for incident mode-i polaritons with frequency ω_I, and from medium to vacuum for scattered mode-j polaritons with frequency ω_S, respectively. Note the factor

$$\left[\frac{\partial\Omega_j^{\rm ext}}{\partial\Omega_j^{\rm int}}\right]=n_j^2\ ,$$

which corrects for the change in solid angle due to refraction. This factor is important in the resonance region where the refractive index n_j depends strongly on frequency. The external RBS cross section thus requires calculations of the internal cross section, the refractive indices (or equivalently the polariton dispersion curves) and transmissivities. We begin by formulating the internal RBS cross section in the next section.

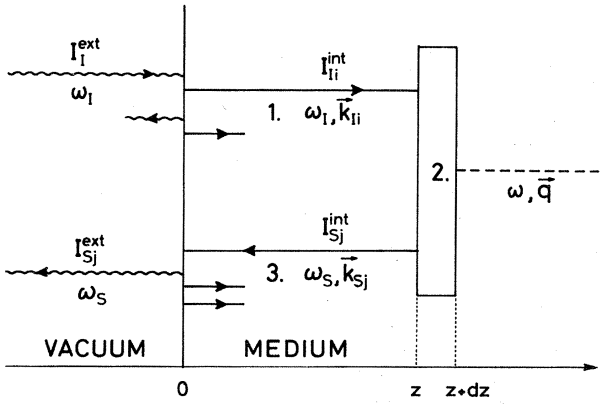

FIG. 3. Schematic representation of a backward RBS experiment using a semi-infinite spatially dispersive medium. Wavy, solid, and dashed lines denote photons, polaritons and acoustic phonons, respectively. The rectangle numbered 2 represents polariton-phonon interactions. Processes numbered 1, 2, and 3 are sequentially occurring events of the internal polariton scattering.

III. SCATTERING CROSS SECTION

As noted before the absorption of polaritons is greatly enhanced in the resonance region. Therefore, in order to calculate the scattering cross section of polaritons we must take the absorption into consideration. This absorption of probe particles (polaritons) causes broadening of the scattered peaks (opaque broadening[14,15]), even if phonon spectra are δ-function-like. In this section we first formulate the internal differential scattering cross section of polaritons by extending the polariton formalism, and then investigate the broadening effect.

A. Scattering Hamiltonian

As shown schematically in Fig. 3, the RBS process inside a medium consists of the following sequence of events: (1) Polaritons are produced at the surface by illuminating it with incident laser light; they travel into the crystal while the intensity decreases gradually. (2) Polaritons are scattered somewhere inside the crystal to the backward direction by emitting or absorbing acoustic phonons. (3) Polaritons come back to the surface, while the intensity again decreases gradually. In this case polaritons are regarded as forced harmonic oscillators with real frequency and complex wave vector. We write $\omega_I,\vec{k}_{Ii}$ and $\omega_S,\vec{k}_{Sj}$ as the frequency and wave vector of incident mode-i and scattered mode-j polaritons, respectively; ω and $\vec{q}$ are the frequency and wave vector of the scattered phonon. The energy-conservation requirement for Brillouin scattering yields

$$\omega_S-\omega_I=\omega\ ,\quad \omega=\pm c_s|q|\ , \tag{3.1}$$

where c_s is the sound velocity. Since polaritons have complex wave vectors, the momentum-conservation rule

$$\vec{k}_{Sj}-\vec{k}_{Ii}=\vec{q}\ , \tag{3.2}$$

does not hold exactly, leading to opaque broadening.

In a spatially homogeneous infinite medium, where the wave vectors which specify polariton states are well-defined quantities, the polariton-phonon interaction Hamiltonian for the backward scattering process numbered 2 in Fig. 3 is given from Eq. (A24) of Appendix A by

$$\mathscr{H}^{ij}_{PL}=V^{-1/2}\sum_q \Gamma_0(q)A_{ij}(k_{Ii},k_{Sj})\delta_{k_{Sj},k_{Ii}+q} \times\alpha^{\dagger}_{k_{Sj}}\alpha_{k_{Ii}}\varphi_q\ , \tag{3.3}$$

where V is the sample volume, A_{ij} is related to the exciton-strength function, and is given by Eq. (A23) in Appendix A, $\Gamma_0(q)$ is the exciton-phonon-interaction kernel, $\varphi_q=i(c_q-c^{\dagger}_{-q})$, and $\alpha^{\dagger}$, α, $c^{\dagger}$, and c are creation and annihilation operators for polaritons and phonons, respectively. For brevity we omit an irrelevant phase factor and subscript z for the z component of momenta in Eq. (3.3), which describes polariton scattering from mode i to mode j by emitting or absorbing a phonon. The substitution of the integral form of Kronecker's δ function which incorporates the momentum-conservation law into Eq. (3.3) yields

$$\mathscr{H}^{ij}_{PL}=\frac{V^{-1/2}}{L}\int_0^L dz\sum_q \Gamma_0(q)A_{ij}(k_{Ii},k_{Sj})\alpha^{\dagger}_{k_{Sj}}(z) \times\alpha_{k_{Ii}}(z)\varphi_q(z)\ , \tag{3.4}$$

where we put $\alpha_k(z)=\alpha_k e^{ikz}$, $\alpha^{\dagger}_k(z)=\alpha^{\dagger}_k e^{-ikz}$, and $\varphi_q(z)=\varphi_q e^{iqz}$. L denotes sample thickness along the z direction; L as well as V will finally be made infinite.

Let us now assume that even in an absorptive semi-infinite medium a slightly modified form of Eq. (3.4) is still valid. We need a few comments to obtain it and to justify the assumption. The attenuation of polaritons is usually attributed to the damping of excitons. When the exciton damping constant Γ is small, the quasiparticle energy $\tilde{\omega}_E(\vec{k},\omega)$ of an exciton is represented by

$$\tilde{\omega}^2_E(\vec{k},\omega)=\omega^2_E(\vec{k})-i\omega\Gamma\ , \tag{3.5}$$

where $\omega_E(\vec{k})$ is the well-defined exciton energy. This relation has been microscopically justified to some extent by Tait[16] by using a Green's-function technique. On the other hand, in Appendix A we obtain the exciton-polariton dispersion equation, Eq. (A8), for the case with $\Gamma=0$. In order to make the theory consistent we should replace $\omega_E(k)$ in Eq. (A8) by $\tilde{\omega}_E(k)$. Then the dispersion equation takes the usual form

$$\frac{c^2k^2}{\omega^2}=\epsilon_b+\frac{4\pi\alpha_0\omega_0^2}{\omega^2_E(k)-\omega^2-i\omega\Gamma}\ , \tag{3.6}$$

where ϵ_b is the background dielectric constant, $\omega_0=\omega_E(0)$ is the transverse exciton frequency at $\vec{k}=\vec{0}$, and α_0 is the polarizability of the exciton. This is exactly the Hopfield-Thomas phenomenological exciton-polariton dispersion equation.[3] As noted before, polaritons in RBS (or RRS) are regarded as forced harmonic oscillators, which means that we must solve Eq. (3.6) for the complex wave vector k for each given real frequency ω. Therefore, in order to use Eq. (3.4) for the RBS problem, we should read k_{Ii},k_{Sj} in the function $A_{ij}(k_{Ii},k_{Sj})$ as $k_{Ii}(\omega_I),k_{Sj}(\omega_S)$, and replace the subscripts k_I,k_S of polariton creation and annihilation operators by ω_I,ω_S, respectively. In other words, the crucial difference of our problem from the usual spatially homogeneous case is that polariton states are specified by frequency instead of wave vector. Therefore, for problems where perturbation theory is applicable the assumption made above is justifiable. Keeping the discussion given above in mind, we have the following scattering Hamiltonian:

$$\mathscr{H}^{ij}_{PL}=V^{-1/2}L^{-1}\int_0^L dz\sum_q \Gamma_0(q)A_{ij}(k_{Ii},k_{Sj}) \times\alpha^{\dagger}_{\omega_{S,j}}(z)\varphi_q(z)\alpha_{\omega_{I,i}}(z)\ . \tag{3.7}$$

B. Transition probability

The rate of transitions associated with Eq. (3.7) is found from time-dependent perturbation theory (golden rule) by

$$\tau^{-1}_{ij}=\frac{2\pi}{\hbar^2}\bar{n}_{Ii}S\sum_{u,f}|\langle f|\mathscr{H}^{ij}_{PL}|u\rangle|^2\delta(\omega+\omega_I-\omega_S)p_u\ , \tag{3.8}$$

where $\bar{n}_{Ii}$ is the number density of mode-i polaritons, L is the sample thickness, S is the surface area illuminated by the incident laser light, $|u\rangle$ and $|f\rangle$ are the initial and final states of the medium associated with the polariton-phonon interaction, and p_u is the initial (equilibrium) phonon probability function. The substitution of the integral form of the δ function in Eq. (3.7), which expresses energy conservation into Eq. (3.8) yields

$$\tau^{-1}_{ij}=\frac{2\pi\bar{n}_{Ii}S}{\hbar^2VL^2}|A_{ij}(k_{Ii},k_{Sj})|^2\int\int dz\,dz'\sum_q\sum_{q'}\frac{1}{2\pi}\int_{-\infty}^{+\infty}dt\,e^{-i\omega t}\sum_{u,f}p_u\langle f|A|u\rangle^*\langle f|B(t)|u\rangle\ , \tag{3.9}$$

where we have set

$$A=\alpha^{\dagger}_{\omega_{S,j}}(z)\Gamma_0(q)\varphi_q(z)\alpha_{\omega_{I,i}}(z)\ , \tag{3.10a}$$

$$B(t)=\alpha^{\dagger}_{\omega_{S,j}}(z')\Gamma_0(q')e^{i\omega_S t}\varphi_{q'}(z') \times e^{-i\omega_I t}\alpha_{\omega_{I,i}}(z')\ . \tag{3.10b}$$

Since initial and final states, $|u\rangle$ and $|f\rangle$, of the medium associated with the polariton-phonon interaction have one polariton with frequencies ω_I and ω_S, respectively (i.e., $\mathscr{H}_P|u\rangle=\hbar\omega_I|u\rangle$, $\mathscr{H}_P|f\rangle=\hbar\omega_S|f\rangle$, where $\mathscr{H}_P$ is the noninteracting polariton Hamiltonian), we have the relation ($\hbar$ has been set equal to 1)

$$\langle f|e^{i\omega_S t}\varphi e^{-i\omega_I t}|u\rangle=\langle f|e^{i\mathscr{H}_P t}\varphi e^{-i\mathscr{H}_P t}|u\rangle$$
$$=\langle f|\varphi(t)|u\rangle\ .$$

Therefore, $B(t)$ can be effectively rewritten as

$$B(t)=\alpha^{\dagger}_{\omega_{S,j}}(z')\Gamma_0(q')\varphi_{q'}(z',t)\alpha_{\omega_{I,i}}(z')\ . \tag{3.10c}$$

Equation (3.9) then takes the form

$$\tau_{ij}^{-1}=\frac{2\pi\bar{n}_{Ii}S}{\hbar^2VL}|A_{ij}(k_{Ii},k_{Sj})|^2\int\int dz\,dz'\sum_q\sum_{q'}\langle A^{\dagger}B\rangle_{\omega}\ , \tag{3.11}$$

where we have used the definition

$$\langle A^{\dagger}B\rangle_{\omega}\equiv\frac{1}{2\pi}\int_{-\infty}^{+\infty}dt\,e^{-i\omega t}\langle A^{\dagger}B(t)\rangle\ . \tag{3.12}$$

Now the well-known fluctuation-dissipation theorem yields the relation[17]

$$\langle A^{\dagger}B\rangle_{\omega}=\frac{2}{1-e^{-\beta\hbar\omega}}\,\mathrm{Im}\langle\langle B;A^{\dagger}\rangle\rangle_{\omega}\ , \tag{3.13}$$

where $\beta=1/k_BT$ and $\langle\langle B;A^{\dagger}\rangle\rangle_{\omega}$ is the Fourier transform of a retarded two-time Green's function;

$$\langle\langle B(t);A^{\dagger}\rangle\rangle\equiv-i\Theta(t)\langle[B(t),A^{\dagger}]\rangle\ ,$$
$$\langle\langle B;A^{\dagger}\rangle\rangle_{\omega}=\frac{1}{2\pi}\int_{-\infty}^{+\infty}dt\,e^{-i\omega t}\langle\langle B(t);A^{\dagger}\rangle\rangle\ . \tag{3.14}$$

The substitution of (3.13) into (3.11) gives

$$\tau_{ij}^{-1}=\frac{2\pi\bar{n}_{Ii}S}{\hbar^2VL^2}|A_{ij}(k_{Ii},k_{Sj})|^2$$
$$\times\int\int dz\,dz'\sum_q\sum_{q'}\frac{2}{1-e^{-\beta\hbar\omega}}\,\mathrm{Im}\langle\langle B;A^{\dagger}\rangle\rangle_{\omega}\ . \tag{3.15}$$

As a first approximation we can separate the polariton part from the two-time Green's function:

$$\langle\langle B;A^{\dagger}\rangle\rangle_{\omega}=\Gamma_0^*(q)\Gamma_0(q')\langle\langle\varphi_{q'}(z');\varphi_q^{\dagger}(z)\rangle\rangle$$
$$\times\langle\alpha^{\dagger}_{\omega_{S,j}}(z')\alpha_{\omega_{I,i}}(z')$$
$$\times\alpha^{\dagger}_{\omega_{I,i}}(z)\alpha_{\omega_{S,j}}(z)\rangle\ . \tag{3.16}$$

Next we assume that the polariton part in Eq. (3.16) can be decomposed into pair products and possible interference effects can be neglected. Since the medium temperature is very low compared with the polariton energy (thermal distribution of polaritons $\langle n_{\mathrm{pol}}\rangle=0$), the thermal average of polaritons can be taken as the ground state with no polaritons, $|g_P\rangle$. Then the polariton part in (3.16) takes the form

$$G_{\omega_{I,i}}(z',z)G_{\omega_{S,j}}(z,z')\ , \tag{3.17}$$

where

$$G_{\omega,i}(z',z)\equiv\langle g_P|\alpha_{\omega,i}(z')\alpha^{\dagger}_{\omega,i}(z)|g_P\rangle \tag{3.18}$$

denotes the probability amplitude that a mode-i polariton with frequency ω is found at z' when it is produced at z. More explicitly $G_{\omega_{I,i}}(z',z)$ can be expressed as

$$G_{\omega_{I,i}}(z',z)=\exp(ik_{Ii}z'-ik_{Ii}^{*}z)\ , \tag{3.19}$$

where $k_{Ii}',k_{Ii}''>0$, while $G_{\omega_{S,j}}(z,z')$ is given by

$$G_{\omega_{S,j}}(z,z')=\exp(ik_{Sj}z'-ik_{Sj}^{*}z)\ , \tag{3.20}$$

where we replaced the scattered momentum by $-k_{Sj}^{*}$ ($k_{Sj}',k_{Sj}''>0$), since as seen in Fig. 3 scattered polaritons travel in the $-z$ direction. On the other hand, the phonon part takes the form

$$\langle\langle\varphi_{q'}(z');\varphi_q^{\dagger}(z)\rangle\rangle_{\omega}=\exp(iq'z'-iqz)D(q',q;\omega)\ , \tag{3.21}$$

where we set

$$D(q',q;\omega)=\langle\langle\varphi_{q'};\varphi_q^{\dagger}\rangle\rangle_{\omega} \tag{3.22}$$

as a retarded two-time Green's function for phonons. Substituting Eqs. (3.16), (3.19), (3.20), and (3.21) into (3.15), we obtain for the transition rate

$$\tau_{ij}^{-1}=\frac{2\pi\bar{n}_{Ii}S}{\hbar^2VL}|A_{ij}(k_{Ii},k_{Sj})|^2$$
$$\times\sum_q\sum_{q'}\frac{2}{1-e^{-\beta\hbar\omega}}\,\mathrm{Im}\frac{\Gamma_0^*(q)\Gamma_0(q')D(q',q;\omega)}{(K_{ij}^{*}+q)(K_{ij}+q')}\ , \tag{3.23}$$

where we set

$$K_{ij}=k_{Ii}+k_{Sj}\ . \tag{3.24}$$

C. Scattering cross section

The amount of energy removed from incident polariton model i per sec due to the scattering process to polariton mode j within ranges of scattered frequency $\omega_S\sim\omega_S+\delta\omega_S$ and solid angle $\Omega_j^{\mathrm{int}}\sim\Omega_j^{\mathrm{int}}+\delta\Omega_j^{\mathrm{int}}$ is

$$\hbar\omega_I\rho_j(\omega_S)\delta\omega_S\delta\Omega_j^{\mathrm{int}}\tau_{ij}^{-1}\ . \tag{3.25}$$

We write I_{Ii} for the mean intensity of the incident mode-i polariton beam at the surface of the medium. The mean intensity of the incident mode-i polariton beam is given by

$$I_{Ii}=\hbar\omega_I v_{Ei}(\omega_I)\bar{n}_{Ii}\ , \tag{3.26}$$

where $v_{Ei}(\omega_I)$ is the energy velocity of the mode-i polariton with frequency ω_I. The internal scattering cross section is given by the ratio of Eqs. (3.25) to (3.26):

$$\frac{\partial^2\sigma_{ij}^{\mathrm{int}}}{\partial\Omega_j^{\mathrm{int}}\partial\omega_S}=\frac{\rho(\omega_S)\tau_{ij}^{-1}}{v_{Ei}(\omega_I)\bar{n}_{Ii}}\ . \tag{3.27}$$

The density of states of mode-j polaritons $\rho_j(\omega_S)$ takes the form

$$\rho_j(\omega_S)=\frac{V}{(2\pi)^3}\frac{(k'_{Sj})^2}{|v_{Gj}(\omega_S)|}, \tag{3.28}$$

where $k'_{Sj}=\mathrm{Re}k_{Sj}$, when the exciton damping constant Γ is sufficiently small so that polaritons can be still be considered to be well defined. Substitution of Eqs. (3.23) and (3.28) into (3.27) gives the expression for the internal scattering cross section

$$\frac{\partial^2\sigma_{ij}^{\mathrm{int}}}{\partial\Omega_j^{\mathrm{int}}\partial\omega_S}=\frac{S}{(2\pi\hbar)^2}\frac{(k'_{Sj})^2|A_{ij}(k_{Ii},k_{Sj})|^2}{v_{Ei}(\omega_I)|v_{Gj}(\omega_S)|}\frac{1}{L}\sum_q\sum_{q'}\frac{2}{1-e^{-\beta\hbar\omega}}\mathrm{Im}\frac{\Gamma_0^*(q)\Gamma_0(q')D(q',q;\omega)}{(K_{ij}^*+q)(K_{ij}+q')}. \tag{3.29}$$

The observable external scattering cross section is obtained by substituting Eq. (3.29) into (2.2),

$$\frac{\partial^2\sigma_{ij}^{\mathrm{ext}}}{\partial\Omega_j^{\mathrm{ext}}\partial\omega_S}=\frac{S}{(2\pi\hbar c)^2}T_i(\omega_I)T'_j(\omega_S)\frac{\omega_S^2|A_{ij}(k_{Ii},k_{Sj})|^2}{v_{Ei}(\omega_I)|v_{Gj}(\omega_S)|}\frac{1}{L}\sum_q\sum_{q'}\frac{2}{1-e^{-\beta\hbar\omega}}\mathrm{Im}\frac{\Gamma_0^*(q)\Gamma_0(q')D(q',q;\omega)}{(K_{ij}^*+q)(K_{ij}+q')}, \tag{3.30}$$

where use was made of the relation $n_j(\omega_S)=ck'_{Sj}/\omega_S$. Note that c in (3.30) is the vacuum light velocity, and not the polariton phase velocity $\bar{c}$ contrary to the erratum of Ref. 11.

The expression (3.30) is still quite general. One can even include boundary effects for phonons,[9] if necessary. However, when the surface effects for phonons are negligible (i.e., polariton attenuation is not too large and the sample thickness L is comparatively large), we can take the phonon Green's function as follows:

$$D(q',q;\omega)=\delta_{q,q'}D(q,\omega),\quad D(q,\omega)=\langle\langle\varphi_q;\varphi_q^\dagger\rangle\rangle_\omega, \tag{3.31}$$

which is the form appropriate for an infinite medium. Let us, moreover, assume that the phonons have no attenuation at all. This approximation is very good for acoustic phonons at low temperatures, as in our case. Then the phonon Green's function can be represented by

$$D(q,\omega)=\frac{2\omega_q}{\omega^2-\omega_q^2},\quad \mathrm{Im}D(q,\omega)=\frac{1}{2c_s}[\delta(\omega/c_s-|q|)-\delta(\omega/c_s+|q|)], \tag{3.32}$$

where c_s is the sound velocity of acoustic phonons under consideration. Substituting Eqs. (3.31) and (3.32) into (3.30) and changing the sum over q to an integral, we obtain for the expression of the external differential scattering cross section

$$\frac{\partial^2\sigma_{ij}^{\mathrm{ext}}}{\partial\Omega_j^{\mathrm{ext}}\partial\omega_S}=\frac{S}{(2\pi)^3(\hbar c)^2c_s}T_i(\omega_I)T'_j(\omega_S)\frac{\omega_S^2|\Gamma_0(K'_{ij})|^2|A_{ij}(k_{Ii},k_{Sj})|^2}{v_{Ei}(\omega_I)|v_{Gj}(\omega_S)|}\times\left[\frac{1+n_{\mathrm{ph}}(\omega_I-\omega_S)}{\left[K'_{ij}-\frac{\omega_I-\omega_S}{c_s}\right]^2+(K''_{ij})^2}+\frac{n_{\mathrm{ph}}(\omega_S-\omega_I)}{\left[K'_{ij}-\frac{\omega_S-\omega_I}{c_s}\right]^2+(K''_{ij})^2}\right], \tag{3.33}$$

where $n_{\mathrm{ph}}(\omega)$ is the Bose-Einstein distribution of phonons,

$$K'_{ij}=\mathrm{Re}K_{ij}=k'_{Ii}+k'_{Sj}$$

and

$$K''_{ij}=\mathrm{Im}K_{ij}=k''_{Ii}+k''_{Sj}.$$

Equation (3.33) shows that if the frequency dependence of all terms except those in the last large parenthesis can be neglected, the scattered light measured outside the medium has a Lorentzian line shape with maxima at

$$\omega_S=\omega_I\pm c_s(k'_{Ii}+k'_{Sj}), \tag{3.34}$$

and full width at half maximum of

$$\Delta=2c_s(k''_{Ii}+k''_{Sj}). \tag{3.35}$$

These results are identical to those obtained by BZB. Equation (3.35) represents opaque broadening[14,15,18] due to the attenuation of polaritons. However, Eqs. (3.34) and (3.35) are correct only when other factors in Eq. (3.33) can be regarded as constant when varying ω_S. In general the transmissivity $T'_j(\omega_S)$ and group velocity $v_{Gj}(\omega_S)$ are strongly varying functions of ω_S. Therefore, in order to discuss the line shape of the scattering light completely, one must evaluate the full expression of (3.33) numerically.

The external scattering cross section per unit solid angle is obtained by integrating the differential scattering cross section of Eq. (3.33) over ω_S. If the exciton damping constant Γ is small, then peaks due to the Lorentzian part in (3.33) are so sharp that other factors can be regarded as constant. Then we find

$$\frac{\partial\sigma_{ij}^{\mathrm{ext}}}{\partial\Omega_j^{\mathrm{ext}}}=\frac{\pi S}{(2\pi)^3(\hbar c)^2}T_i(\omega_I)T'_j(\omega_S)\frac{\omega_S^2|\Gamma_0(K'_{ij})|^2|A_{ij}(k_{Ii},k_{Sj})|^2}{v_{Ei}(\omega_I)|v_{Gj}(\omega_S)|K''_{ij}}\times\begin{cases}1+n_{\mathrm{ph}}(\omega_I-\omega_S)\ \text{(Stokes)}\\ n_{\mathrm{ph}}(\omega_S-\omega_I)\ \text{(anti-Stokes)}.\end{cases} \tag{3.36}$$

The factor $(K_{ij}'')^{-1}=(k_{Ii}''+k_{Sj}'')^{-1}$ represents phenomenologically an effective scattering length due to the attenuation of polaritons. [The effective scattering volume is $S/(K_{ij}'')$.]

IV. NUMERICAL CALCULATIONS OF RBS SCATTERING EFFICIENCY

Various quantities such as transmissivities, energy, and group velocities, etc., contained in the RBS efficiency, Eq. (3.36) derived in the preceding section, are expected to exhibit strong frequency dependence in the resonance region. In this section we first analyze the quantitative behavior of the above properties separately, and finally join the properties to obtain the internal and external scattering cross sections. By doing so one can check which factors are responsible for the characteristic structure of the external scattering cross section.

A. Exciton-polariton dispersion curves

First of all we use the Hopfield-Thomas exciton-polariton dispersion equation, (3.6), introduced in the preceding section. The exciton frequency is

$$\omega_E(k)=\omega_0+\hbar k^2/2m^* ,$$

where m^* is an effective exciton mass. For small values of wave vector $\vec{k}$ in the Brillouin zone, we can set

$$\omega_E^2(k)=\omega_0^2+(\hbar\omega_0/m^*)k^2 . \tag{4.1}$$

In the dispersion equation (3.6), we neglected frequency-dependent contributions from other excitons (the background dielectric constant ϵ_b is assumed to be a frequency-independent constant). In other words, we assume a single parabolic exciton band immersed in a background with constant ϵ_b. In CdS the frequency-dependent contribution from the B exciton is known to be small near ω_0 of the A exciton. As discussed in the preceding section our experimental situation in RBS (Fig. 3) imposes the condition that frequency ω is real and wave vector $\vec{k}$ is complex (forced harmonic-oscillator picture in Ref. 16), i.e., we must solve Eq. (3.6) for $\vec{k}$ with a given real ω.

Numerical solutions of the exciton-polariton dispersion equation (3.6) with (4.1) are shown in Fig. 4 for various values of the exciton damping parameter Γ. The refractive index n_i and extinction coefficient κ_i of mode-i polaritons are obtained from

$$n_i(\omega)=ck_i'(\omega)/\omega , \quad \kappa_i(\omega)=ck_i''(\omega)/\omega , \tag{4.2}$$

where k' and k'' are the real and imaginary parts of the polariton wave vector. [Note that in all figures we use the conventional unit of cm^{-1} for numerical calculations (see the beginning of Appendix B). Therefore, use is made of wave numbers instead of wave vectors in all figures.] The most striking aspect of this figure is the existence of a threshold value of the exciton damping constant, Γ_c, given by

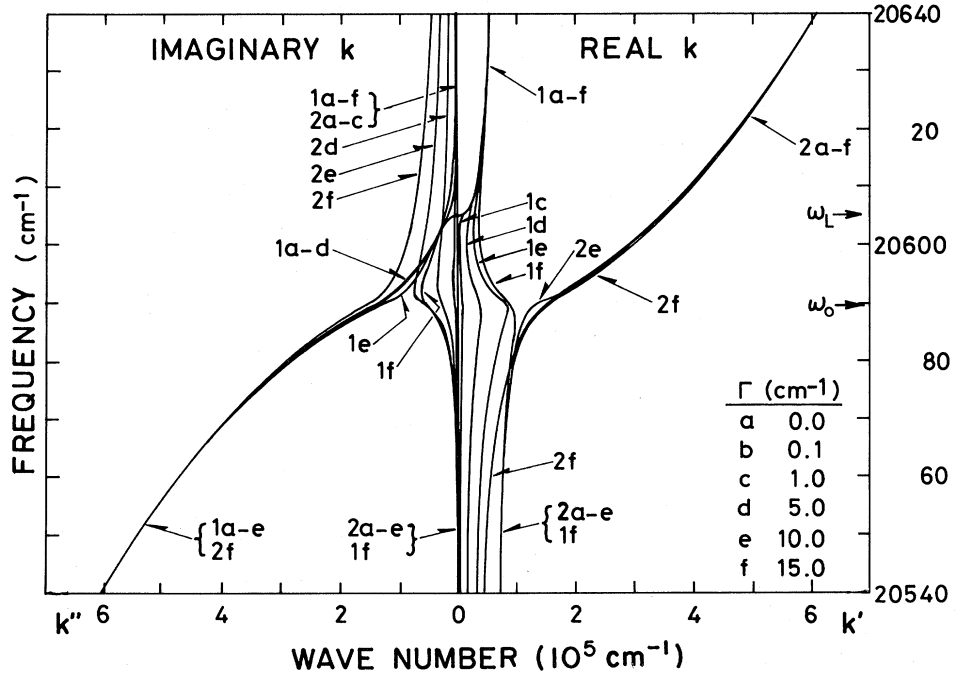

FIG. 4. Numerical solutions of the exciton-polariton dispersion equation (3.6), of the A exciton in CdS for various values of the exciton damping constant Γ. k', the real part of k, is shown on the right-hand side of the figure and k'', the imaginary part of k, on the left-hand side. ω_0 and ω_L are, respectively, the transverse and longitudinal exciton frequencies at the center of the Brillouin zone. The numbers 1 and 2 denote specific polariton modes while small letters denote specific values of Γ (a, 0.0; b, 0.1; c, 1.0; d, 5.0; e, 10.0; f, 15.0 cm^{-1}), e.g., $2c$ indicates a real or imaginary wave number of mode-2 polariton with $\Gamma=1.0$ cm^{-1}. Note the drastic change of the curves when $\Gamma\gtrsim\Gamma_c$ ($=11.5$ cm^{-1}). The parameter values used are $\epsilon_b=9.3$, $4\pi\alpha_0=0.0139$, $\omega_0=20\,589.5$ cm^{-1}, and $m^*/m_e=0.89$.

$$\Gamma_c^2 = 4AB\omega_0^2 , \tag{4.3}$$

where $A = 4\pi\alpha_0$ and $B = \hbar\omega_0/m^*c^2$ (Appendix B is assigned to the derivation). As pointed out first by Tait,[16] it is characteristic of the forced harmonic-oscillator picture. While below Γ_c all the curves are very similar to the one with $\Gamma = 0$ (the usual polariton dispersion curve), for $\Gamma \gtrsim \Gamma_c$ the curves change drastically and the resulting curves of the two polariton modes cross each other looking similar to pure photons (mode 1) and excitons (mode 2), as if there were no interaction between them. As shown later, due to this behavior the scattering efficiency curves change qualitatively for Γ near Γ_c. In the case of the A exciton in CdS, $\Gamma_c = 11.5\ \text{cm}^{-1}$ for the values of the parameters indicated in Fig. 4.

B. Scattered frequency

Owing to inherent opaqueness of a medium near its resonance region we must use the backward scattering geometry. The energy- and momentum-conservation laws, Eqs. (3.1) and (3.2), enable us to calculate the RBS frequency ω_S as a function of incident laser frequency ω_I, although Eq. (3.2) holds only approximately in this case. The kinematics of backward RBS is shown in Fig. 1 by arrows. The scattered frequency ω_S from mode-i initial to mode-j final polaritons is given by

$$\omega_S = \omega_I + \epsilon c_s[k_i'(\omega_I) + k_j'(\omega_S)] \tag{4.4}$$

[see also Eq. (3.34)], where c_s is the sound velocity of acoustic phonons and ϵ takes the value -1 for Stokes and $+1$ for anti-Stokes scattering. One must solve Eq. (4.4) numerically by an iterative method, since k_j' on the right-hand side includes ω_S. Figure 2 shows one example of the curves of ω_S as a function of ω_I. Note the striking similarity of profile to the exciton-polariton dispersion curves in Fig. 1. It is this resemblance which gives RBS experiments their principle advantage for studying the properties of exciton polaritons. One can determine the parameters ω_0, ϵ_b, α_0, and m^* very accurately and almost independently from each other by plotting the RBS frequency data and adjusting the parameters to fit the theoretical curves to the data, since different parts of the ω_S curve (or dispersion curve) are most sensitive to changes of each parameter. When m^* is changed, only the curvature of the excitonlike part of the curve will change, and the other parts will remain essentially unchanged. As is easily seen from Fig. 4, the ω_S curves are insensitive to the value of Γ when $\Gamma < \Gamma_c$.

C. Transmissivities

In a polarizable medium, one can in general have more than two polariton modes for one specific frequency due to the finite mass of excitons. Therefore, one must incorporate appropriate ABC's. As mentioned earlier we restrict ourselves to the single-oscillator exciton-polariton model indicated in Fig. 1, bearing in mind that we will apply our results only to the A exciton in CdS. In other words, we have two independent polariton modes in the spatially dispersive medium.

Making reference to Fig. 3, Maxwell's boundary conditions are expressed for the normal incidence case as follows:

$$E_{I0} + E_{R0} = E_{T1} + E_{T2} , \tag{4.5}$$

$$E_{I0} - E_{R0} = n_{c1}E_{T1} + n_{c2}E_{T2} , \tag{4.6}$$

where E_{I0} and E_{R0} are electric field amplitudes of incident and reflected photons just outside the medium, and E_{T1} and E_{T2} are the amplitudes of the transmitted mode -1 and -2 polaritons just inside the medium with complex refractive indices n_{c1} and n_{c2}, respectively ($n_{cj} = n_j + i\kappa_j$; $j = 1$ or 2). Because of the additional mode on the right-hand side of Eqs. (4.5) and (4.6) one ABC is required in order to obtain unique reflectivity and transmissivity expressions.

A brief review of the origin of the three most frequently discussed ABC's will now be given. The first ABC (called ABC1), given by Pekar,[1] is based on the condition that the total excition polarization must vanish at the crystal boundary

$$\sum_{i=1}^{2} P_{\text{ex}_i} = 0 \text{ at } z = 0 ,$$

where the z axis is perpendicular to the crystal surface, and P_{ex_i} denotes the exciton polarization associated with the ith transmitted wave. Pekar asserted that this should be the ABC to supplement the Maxwell boundary conditions after showing that the crystal boundaries turned out to be nodal surfaces for the exciton wave function as well as for the dipole moment associated with the exciton.

Subsequently, Birman and Sein,[19] Maradudin and Mills,[20] Agarwal *et al.*,[21] and others[22,23] independently explored the ABC problem starting from Maxwell's equations rather than from a phenomenological approach. These groups discovered that once a particular nonlocal susceptibility is chosen, the resulting ABC can be determined through either an integral or differential equation formulation of the electrodynamics of the nonlocal medium with no further assumptions being necessary. For example, when the dielectric approximation for the susceptibility is chosen, the resulting (ABC3) is[19–21]

$$\sum_{i=1}^{2} \frac{P_{\text{ex}_i}}{(n_{c_i} - n_e)(n_{c_i}^2 - \epsilon_b)} = 0 \text{ at } z = 0 ,$$

where n_{c_i} is the refractive index of the ith transmitted polariton mode, ϵ_b is a background dielectric constant, and n_e is just the refractive index for the uncoupled exciton, the explicit expression of which is given in Eq. (4.9).

A more microscopic approach for finding ABC's was given by Zeyher *et al.*[24] This approach suggested that different ABC's for exciton polaritons can arise from different assumptions about the reflection of an exciton at the crystal surface. Ting *et al.*[25] showed that for Wannier excitons the following ABC results (ABC2):

$$\sum_{i=1}^{2} n_{c_i} P_{\text{ex}_i} = 0 \text{ at } z = 0 .$$

Although the ABC is macroscopically concerned with

the boundary condition of the polarization due to the exciton, P_{ex}, we can always rewrite it in terms of the electric field amplitude of polaritons. Here, following Ref. 4, we consider the three representative ABC's. They are conveniently expressed as follows:

$$a_1 E_{T1} + a_2 E_{T2} = 0 , \tag{4.7}$$

where a_j $(j=1,2)$ takes the form (for ABC1, ABC2, and ABC3, respectively)

$$a_j = \begin{cases} n_{cj}^2 - \epsilon_b , \\ n_{cj}(n_{cj}^2 - \epsilon_b) , \\ (n_{cj} - n_e)^{-1} , \end{cases} \tag{4.8}$$

and

$$n_e = \frac{1}{\omega}\left[\frac{\omega^2 - \omega_0^2 + i\omega\Gamma}{B}\right]^{1/2} . \tag{4.9}$$

Next, let us define transmissivity as the ratio of the time average of transmitted energy flow to that of incident energy flow.[26] Since the time average of the energy flow is given by the real part of the time average of the Poynting's vector,[27] transmissivity T and reflectivity R are defined as

$$T \equiv \frac{\mathrm{Re}\bar{S}_T}{\mathrm{Re}\bar{S}_I} , \quad R \equiv \frac{\mathrm{Re}\bar{S}_R}{\mathrm{Re}\bar{S}_I} , \tag{4.10}$$

where $\bar{S}_I$, $\bar{S}_T$, and $\bar{S}_R$ are the time average of the Poynting's vector of incident, transmitted, and reflected energy flows, respectively. As is well known we have $\bar{S}_I = (c/8\pi)\,|E_{I0}|^2$ in vacuum. In the polarizable medium the calculation of Poynting's vector is not so trivial: If the exciton effective mass is infinite $(m^* = \infty)$, then the polariton energy is carried only by electromagnetic waves, since excitons do not move.[27] If the effective mass is finite, however, the energy is carried not only by electromagnetic waves but also by mobile excitons (polarization waves). With the use of the generalized Poynting's theorem[16,28] and the argument by Loudon,[27] we obtain

$$\mathrm{Re}\bar{S}_{Ti} = \frac{cn_i}{8\pi}\frac{\Gamma}{\Gamma - 2B\omega n_i \kappa_i}\,|E_{Ti}|^2 , \tag{4.11}$$

for mode-i $(i=1$ or 2) transmitted polaritons. The Poynting's vector contains contributions from both electromagnetic and polarization waves. Transmissivities from vacuum to medium for each mode and reflectivity are obtained from Eq. (4.5)–(4.11),

$$T_1 = \frac{n_1\Gamma}{\Gamma - 2B\omega n_1\kappa_1}\left|\frac{2a_2}{a_2(1+n_{c1}) - a_1(1+n_{c2})}\right|^2 , \tag{4.12a}$$

$$T_2 = \frac{n_2\Gamma}{\Gamma - 2B\omega n_2\kappa_2}\left|\frac{2a_1}{a_2(1+n_{c1}) - a_1(1+n_{c2})}\right|^2 , \tag{4.12b}$$

$$R = \left|\frac{a_2(1-n_{c1}) - a_1(1-n_{c2})}{a_2(1+n_{c1}) - a_1(1+n_{c2})}\right|^2 . \tag{4.12c}$$

Recently, Nakayama has developed the theory of the quantization of polariton fields for the nonabsorbing $(\Gamma = 0)$ bounded semiconductor.[29] One direct consequence of his treatment is the reciprocity relation for the transmissivities

$$T_i'(\omega) = T_i(\omega) , \tag{4.13}$$

which means that the energy flux ratio associated with mode-i polaritons from crystal into vacuum is the same as that from vacuum into crystal. From this point on we use this relation even for the absorbing $(\Gamma \neq 0)$ medium.

Figure 5 shows numerical results of transmissivities [(4.12a), and (4.12b)] of incident light for the three ABC's (4.8). As expected, the curves for different ABC's coincide with each other, both well below ω_0 and well above ω_L. Prominent and qualitative features are the existence of a peak near ω_L for the mode-2 transmissivity and the peak height difference among the different ABC's. According to detailed numerical analysis the height of the peak decreases gradually when Γ is increased and disappears when $\Gamma \sim \Gamma_c$; instead a new peak appears near ω_0 and grows drastically for all ABC's, reflecting the quick deformation of the dispersion curves near ω_0 when $\Gamma \sim \Gamma_c$ in Fig. 4. The result for ABC1 is qualitatively similar to that obtained by Sel'kin.[28] In Fig. 6 we show the transmissivity product $T_2(\omega_I)T_2'(\omega_S)$ as a function of incident frequency ω_I for various ABC's by incorporating the kinematics of RBS for the LA phonon in CdS. The shoulders on the high-frequency side of the prominent peaks near ω_L are due to peaks which appear in $T_2'(\omega_S)$ when $\omega_S \sim \omega_L$.

D. Group and energy velocities

The group velocity for mode-i polaritons is defined by $v_{Gi} = (dk_i'/d\omega)^{-1}$. The group velocity can be calculated

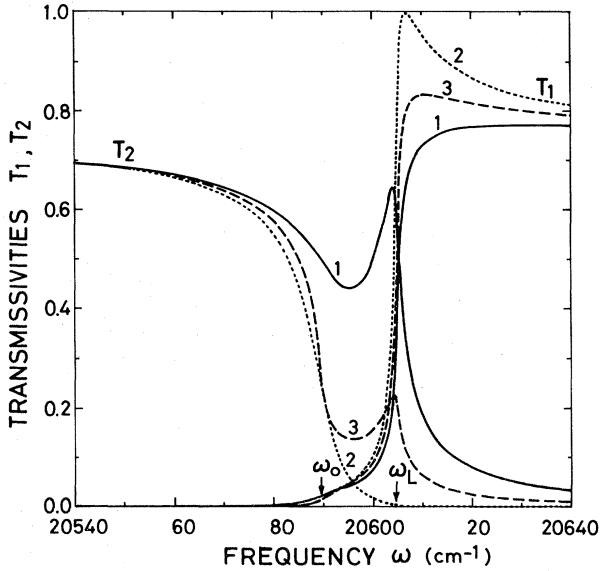

FIG. 5. Numerically calculated transmissivities of mode-1 and -2 polaritons from vacuum to medium for various ABC's as a function of frequency. The number labeled on each curve specifies the ABC used to calculate it (1, ABC1; 2, ABC2; 3, ABC3). The parameter values used are the same as those in Fig. 4 with $\Gamma = 1.0\ \mathrm{cm}^{-1}$.

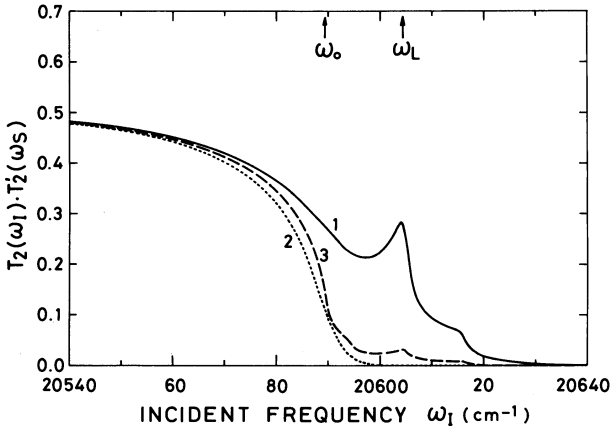

FIG. 6. Product of transmissivities of the incident mode-2 and scattered mode-2 polaritons, $T_2(\omega_I)T_2'(\omega_S)$, as a function of incident laser frequency ω_I. RBS kinematics has been used in the calculation of the scattered polariton frequency ω_S. The number labeled on each curve has the same meaning as in Fig. 5. The parameter values used are the same as those in Fig. 4 with $\Gamma=1.0\ \text{cm}^{-1}$.

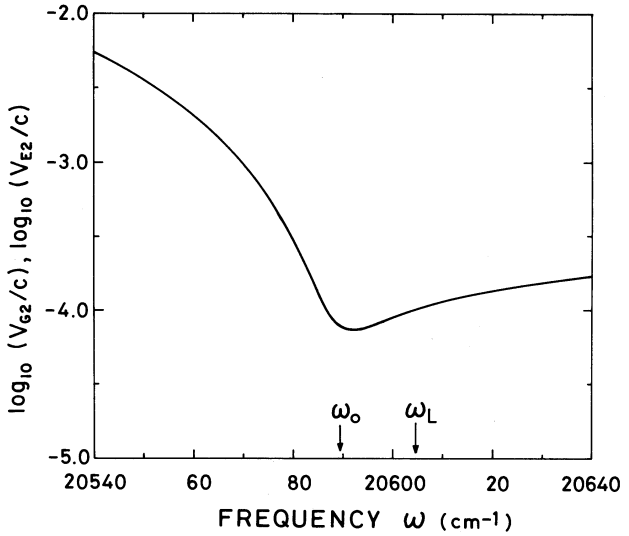

FIG. 7. Group and energy velocities (normalized by light velocity) of mode-2 exciton polaritons plotted on a logarithmic scale, $\log(v_{G2}/c)$ and $\log(v_{E2}/c)$, as a function of frequency ω. One cannot see any visible difference between the two. Maximum value of the relative difference $|v_{E2}-v_{G2}|/v_{E2}$, which occurs at $\omega\cong 20584\ \text{cm}^{-1}$ just below ω_0 when $\Gamma=1.0\ \text{cm}^{-1}$, is only 2.8×10^{-3}. The parameter values used are the same as those in Fig. 4 with $\Gamma=1.0\ \text{cm}^{-1}$.

numerically either from the dispersion curves (Fig. 4) or by laborious evaluation of the analytic formula. The energy velocity v_E, on the other hand, is defined by[27] $v_E=\bar{S}_t/\bar{W}_t$, where $\bar{S}_t$ and $\bar{W}_t$ are, respectively, the time average of the total Poynting's vector and energy density with contributions from both electromagnetic and polarization waves.[27] They are again calculated by using the generalized Poynting's theorem,[16,28] and the energy velocity of mode-i polaritons is given by

$$v_{Ei}(\omega)=c\left[n_i+\frac{2\omega\kappa_i}{\Gamma}+\frac{2B\omega\kappa_i}{\Gamma}(\kappa_i^2-n_i^2)\right]^{-1}, \tag{4.14}$$

where $n_i=ck_i'/\omega$ and $\kappa_i=ck_i''/\omega$ are obtained from the dispersion curves (Fig. 4). In Fig. 7 we show numerical results of both group and energy velocities of mode-2 (outer-branch) polaritons as a function of frequency ω. One cannot see any difference between the two for the parameter values used, although numerically there exists a very small difference which gets larger when ω approaches ω_0 and Γ is increased. Detailed numerical calculations indicate that the curves are very insensitive to Γ values when $\Gamma<\Gamma_c$.

E. Exciton-strength function

The exciton-strength function represents the fraction of exciton character in the polariton mode. If there is no exciton damping ($\Gamma=0$), one can obtain the exciton-strength function quantum mechanically,[11] as derived in Appendix A, Eq. (A23b). Otherwise, one must resort to a phenomenological approach. Extending the idea of Mills and Burstein[30] to the spatial dispersion case, we obtain the exciton-strength function $A_i(k_i)$ for mode-i polaritons

$$A_i(k_i)=\frac{2\kappa_i\omega_E(k_i)}{\Gamma-2B\omega n_i\kappa_i}\left[n_i+\frac{2\omega\kappa_i(1+B\kappa_i^2)}{\Gamma-2B\omega n_i\kappa_i}\right]^{-1} \tag{4.15}$$

Equation (4.15) can be derived by taking the ratio of the mean-square exciton polarization associated with a polariton of frequency $\omega_i(\vec{k})$ to the mean-square exciton polarization associated with an exciton of frequency $\omega_{ex}(\vec{k})$. The numerator of this ratio can be obtained from the total energy density of the polariton (both the mechanical and electromagnetic contributions). The denominator is similarly obtained from the mechanical (exciton) energy density.

From Eq. (4.15) one can recover both the Mills and Burstein result by setting $B=0$ and $\omega_E=\omega_0$ (nonspatial dispersion case: $m^*=\infty$) and the quantum-mechanical result by setting $\Gamma=0$ (zero-absorption case). Figure 8 shows the variation of the exciton-strength function for both polariton modes as a function of frequency (note the ordinate scale). It has no "resonance" effect at all and the numerical variation is very small even in the resonance region. Detailed numerical analysis indicates that the exciton-strength function is very insensitive to Γ values when $\Gamma<\Gamma_c$.

F. Internal scattering cross section

We have now finished preparing the numerical calculations required for the internal scattering cross section, which is just the observable external scattering cross section (3.36) without the transmissivity and solid angle correction factors;

$$\frac{\partial\sigma_{ij}^{\text{int}}}{\partial\Omega_j^{\text{int}}}=\frac{S}{8\pi^2\hbar^2}\frac{(k_{Sj}')^2\,|\,\Gamma_0(q)\,|^2\,|\,A_{ij}(k_{Ii},k_{Sj})\,|^2}{v_{Ei}(\omega_I)\,|\,v_{Gj}(\omega_S)\,|\,K_{ij}''}$$
$$\times[1+n_{\text{ph}}(\omega_I-\omega_S)], \tag{4.16}$$

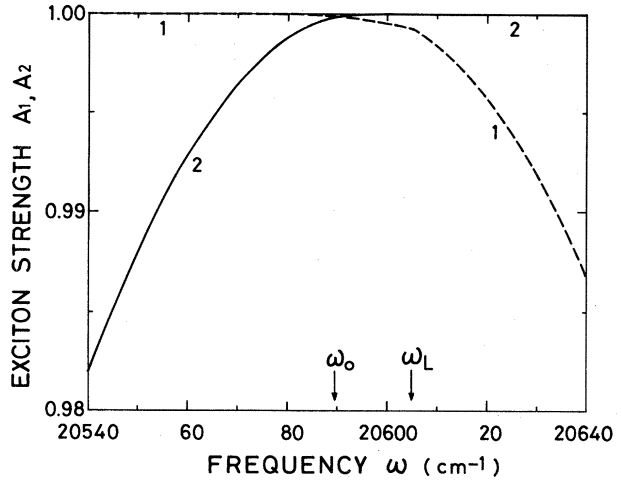

FIG. 8. Exciton-strength functions of both mode-1 and -2 polaritons as a function of frequency. The number labeled on each curve specifies the polariton mode. Note the ordinate scale. The parameter values used are the same as those in Fig. 4 with $\Gamma=1.0\ \mathrm{cm}^{-1}$.

where $K_{ij}''=k_{Ii}''+k_{Sj}''$. This cross section, which is equivalent to that discussed by Burstein *et al.*,[11] does not include the ABC. We want to compare the internal scattering cross section with the external one and point out how important the transmissivity and solid angle correction factors are to the complete scattering cross section. This fact demonstrates the great advantage of RBS in determining the proper ABC experimentally.

For a medium with hexagonal symmetry (e.g., wurtzite CdS with C_{6v} symmetry), only the LA phonon will be allowed in Brillouin backscattering via the deformation-potential interaction. In this case, the exciton-phonon-interaction kernel for the deformation-potential interaction is given by

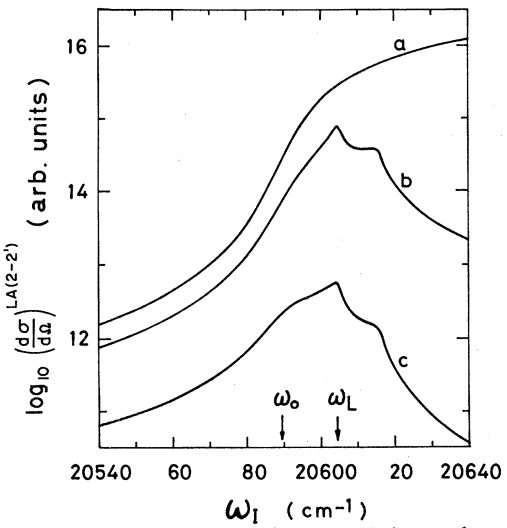

FIG. 9. Curve *a*, variation of the RBS internal; curve *b*, external without solid angle correction factor; and curve *c*, observable external scattering cross sections for the LA Stokes (2-2') scattering plotted on a logarithmic scale as a function of incident laser frequency ω_I. ABC1 is assumed for curves *b* and *c*. The parameter values are the same as those in Fig. 4 with $\Gamma=1.0\ \mathrm{cm}^{-1}$ and $T=4.2$ K.

TABLE I. Values used in the expressions for the deformation potential and piezoelectric interactions.

Sound velocities[a]	
	$c_{s\mathrm{LA}}=4.25\times10^5$ cm/sec
	$c_{s\mathrm{TA}}=1.76\times10^5$ cm/sec
Crystal density[a]	
	$\rho=4.84$ g/cm^3
Piezoelectric constant[b]	
	$e_{15}=-0.21$ C/m^2
Deformation potentials[c]	
	$D_e=4.5$ eV
	$D_h=-2.9$ eV
A-exciton Bohr radius[d]	
	$a_B=28$ Å
Effective hole mass[e]	
	$m_h^*=0.7m_e$
Effective electron mass[f]	
	$m_e^*=0.2m_e$
Background dielectric constant[e]	
	$\epsilon_b=9.3$

[a] D. Gerlich, J. Phys. Chem. Solids 28, 2575 (1967).
[b] A. R. Huston, J. Appl. Phys. 32, 2287 (1961).
[c] D. W. Langer, R. N. Euwena, K. Era, and T. Koda, Phys. Rev. B 2, 4005 (1970).
[d] J. J. Hopfield and D. G. Thomas, Phys. Rev. 122, 35 (1961).
[e] G. Winterling and E. S. Koteles, in *Lattice Dynamics*, edited by M. Balkanski (Flammarion, Paris, 1978), p. 170.
[f] D. G. Thomas and J. J. Hopfield, Phys. Rev. 116, 573 (1959).

$$\Gamma_0^{\mathrm{DP}}(q)=(\hbar/2\rho c_{s\mathrm{LA}})^{1/2}\sqrt{q}\,(D^e+D^h)\ , \tag{4.17}$$

where ρ is the crystal density, $c_{s\mathrm{LA}}$ is the longitudinal sound velocity and D^e (D^h) is the deformation potential for the electron (hole).

However, in piezoelectric crystals such as CdS, TA phonons can also participate in backward scattering via the piezoelectric exciton-phonon interaction.[31] This interaction is similar to the Fröhlich interaction between excitons and LO phonons. The exciton-phonon-interaction kernel in Eq. (4.16) for TA scattering is given by

$$\Gamma_0^{pe}(q)=\frac{2\pi e a_B^2}{\epsilon_b}e_{15}\left[\frac{\hbar}{2\rho c_{s\mathrm{TA}}}\right]^{1/2}q^{3/2}\frac{m_e^*-m_h^*}{m_e^*+m_h^*}\ . \tag{4.18}$$

Here a_B is the exciton Bohr radius, e_{15} is the relevant piezoelectric tensor component, ϵ_b is the background dielectric constant, $c_{s\mathrm{TA}}$ is the TA sound velocity, and m_e^* (m_h^*) is the effective electron (hole) mass. Appropriate CdS values for these two exciton-phonon interactions are listed in Table I.

Figure 9 shows the internal scattering cross section

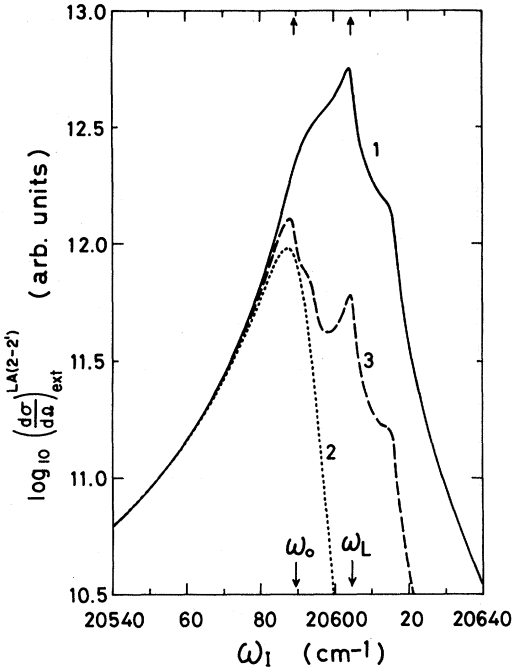

FIG. 10. Variation of the RBS external scattering cross section for the LA Stokes (2→2′) scattering channel for various ABC's on a logarithmic scale as a function of incident laser frequency ω_I. The number labeled on each curve denotes the specific ABC (see Fig. 5). The parameter values used are the same as those in Fig. 4 with $\Gamma=1.0$ cm^{-1} and $T=4.2$ K.

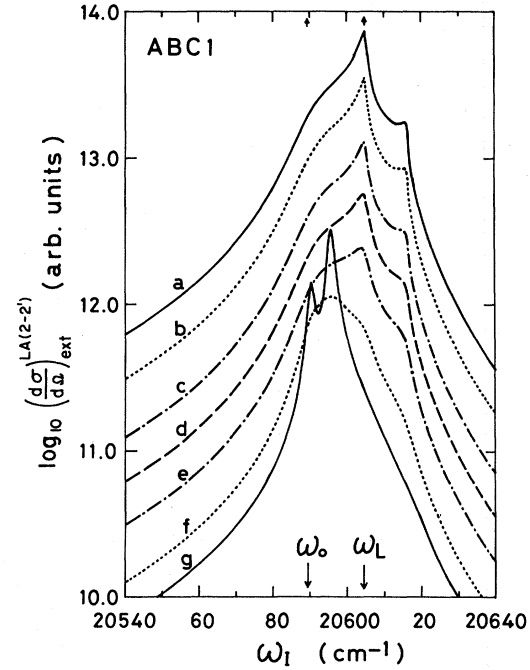

FIG. 11. Variation of the RBS external scattering cross section for the Stokes (2→2′) scattering channel for various Γ values on a logarithmic scale as a function of incident laser frequency ω_I. The letters labeled on each curve denote specific values of Γ (*a*, 0.1; *b*, 0.2; *c*, 0.5; *d*, 1.0; *e*, 2.0; *f*, 5.0; *g*, 10 cm^{-1}). ABC1 is used. The parameter values used are the same as those in Fig. 4 with $T=4.2$ K.

(curve *a*), the external cross section without the solid angle correction factor $n_2^{-2}(\omega_S)$ (curve *b*), and the observable external cross section (curve *c*), for LA Stokes (2→2′) scattering. For curves *b* and *c*, ABC1 was used. The internal cross section has a rather simple monotonic increase with incident frequency ω_I, although the rate of increase becomes large near ω_0. This rapid increase comes from the factors $\Gamma_0(q)$, $(k'_{S2})^2$, and the energy and group velocities in Eq. (4.16), as seen in Figs. 4 and 7. Comparing Fig. 9 with Fig. 6 one can conclude that the prominent structure in the observable external scattering cross section (curve *c*) comes mainly from the transmissivity factor in Eq. (3.36). The solid angle correction factor is also very important, since as seen from the figure, the relative peak heights and overall profile are altered crucially by it. As expected from the outer branch (mode 2) of the dispersion curves in Fig. 4 this factor suppresses the scattering efficiency curves more strongly at higher incident frequency as seen from curve *b* to curve *c*. Detailed numerical analysis indicates that the medium temperature T has little effect on the overall cross-section curve profile from 0 to 4.2 K. Curve *c* (external scattering cross section) for other ABC's will be shown in the next section.

G. External scattering cross section

Finally, we show numerical calculation results of the observable external scattering cross section $\partial\sigma_{ij}^{ext}/\partial\Omega_j^{ext}$. From Eqs. (3.36) and (4.16) it is expressed as

$$\frac{\partial\sigma_{ij}^{ext}}{\partial\Omega_j^{ext}}=\frac{T_i(\omega_I)T'_j(\omega_S)}{n_j^2(\omega_S)}\frac{\partial\sigma_{ij}^{int}}{\partial\Omega_j^{int}}\,, \tag{4.19}$$

for mode-i to -j polariton scattering. Since we have already calculated all the factors on the right-hand side of

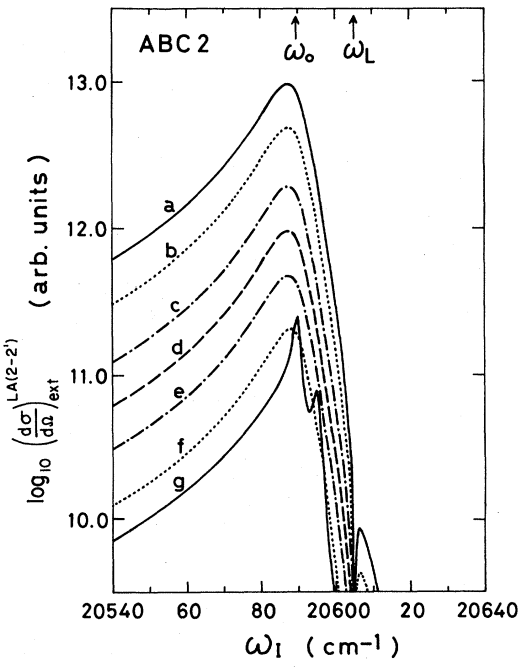

FIG. 12. Same as Fig. 11 except that ABC2 is used.

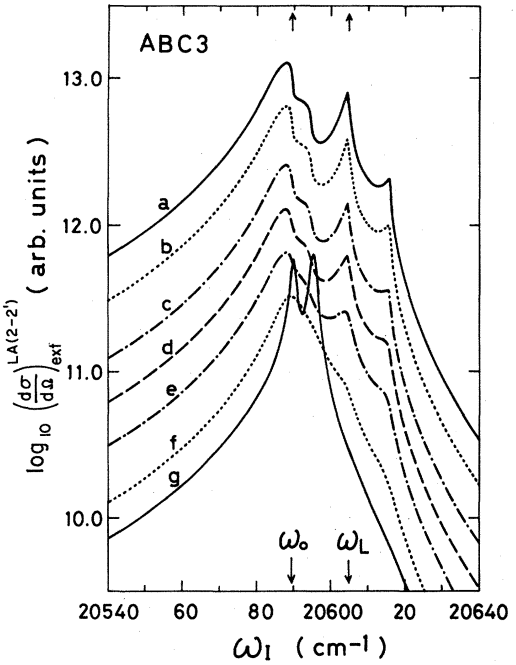

FIG. 13. Same as Fig. 11 except that ABC3 is used.

Eq. (4.19), we have only to join the results obtained in the previous sections to obtain the external scattering cross section. Owing to the transmissivity factors in (4.19) one now has effects of the choice of ABC's, as we have seen in Fig. 9. (In Figs. 9—16 the ordinate scale is arbitrary, but all these figures have identical scales.)

In Fig. 10 (see, also, I, Figs. 8 and 9 for LA and TA scattering, respectively, with $\Gamma=0.5$ cm^{-1}) the variation of the external scattering cross section for LA Stokes (2-2′) scattering is shown as a function of incident laser frequency ω_I, computed for the three ABC's but with fixed exciton damping constant ($\Gamma=1.0$ cm^{-1}). One clearly sees qualitative differences among the curves for different ABC's. A peak near ω_L on the curves for ABC1 and ABC3 comes from the peak appearing on the transmissivity curves in Fig. 5. The peak on the curve for ABC3 is more prominent than that for ABC1, because the peak on the transmissivity curve for ABC3 is relatively more prominent. Note that while a sharp drop appears once near ω_L for ABC1 and near ω_0 for ABC2, it appears twice near ω_0 and ω_L for ABC3. Well below ω_0 all three curves coincide, as expected. Thus, the sharp increase below ω_0 comes mainly from the resonance effect of the internal scattering cross section, while the characteristic structures near ω_0 and ω_L are due to the transmissivity factor (or ABC), and the drop above ω_0 or ω_L is partly due to the transmissivity factor and partly due to the solid angle correction factor $n_2^{-2}(\omega_S)$.

The next three figures, Figs. 11—13, show the variation of the external scattering cross section with various values

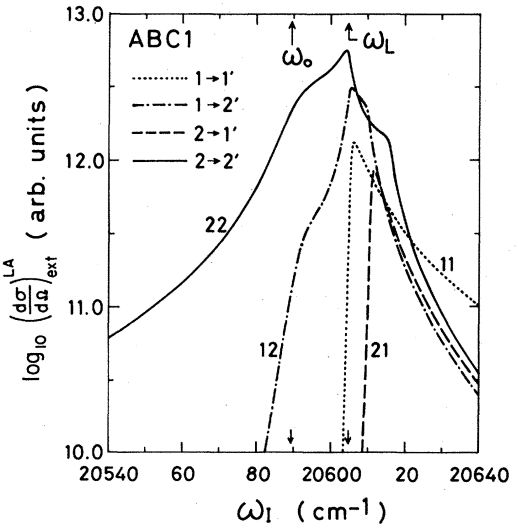

FIG. 14. Variation of the RBS external scattering cross section for the four Stokes scattering channels on a logarithmic scale as a function of incident laser frequency ω_I. Dotted, dashed-dotted, dashed, and solid lines denote 1→1′, 1→2′, 2→1′, and 2→2′ scattering channels, respectively. Only ABC1 is used. The parameter values used are the same as those in Fig. 4 with $\Gamma=1.0$ cm^{-1} and $T=4.2$ K.

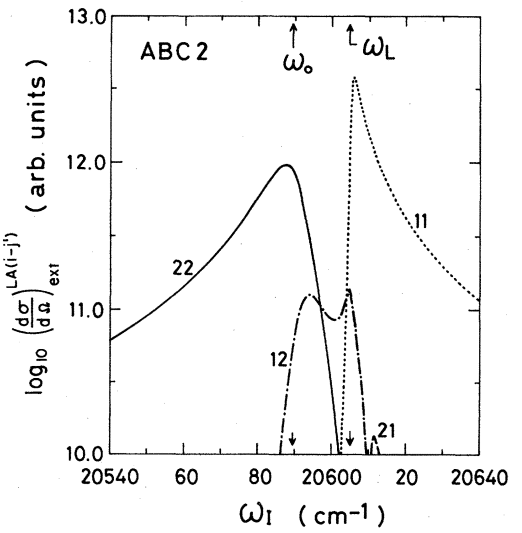

FIG. 15. Same as Fig. 14 except that ABC2 is used.

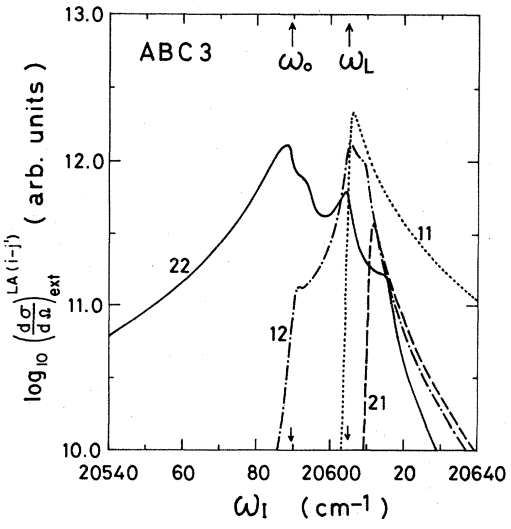

FIG. 16. Same as Fig. 14 except that ABC3 is used.

of the exciton damping constant Γ for LA Stokes (2-2′) scattering for three ABC's, respectively. Note that the threshold value Γ_c is 11.5 cm^{-1}. While well below Γ_c (i.e., $\Gamma < 0.5\Gamma_c$) the curves are rather insensitive to the change of Γ values for all three ABC's, a sudden qualitative change of profile occurs for Γ near Γ_c. This is entirely due to the qualitative change of the dispersion curves near Γ_c in Fig. 4, which also causes significant change of the transmissivity curves: The sharp peak at ω_0 on the curves with $\Gamma = 10.0$ cm^{-1} ($\sim\Gamma_c$) for each ABC, comes from the same origin as the peak appearing on the transmissivity curve; it appears when $\omega_I \cong \omega_0$. Another sharp peak just above ω_0 appears when $\omega_S \cong \omega_0$. We want to point out here that although our method is quite different from BZB's, our scattering cross-section curves with $\Gamma = 10$ cm^{-1} for all three ABC's are qualitatively very similar to those obtained by BZB for which they used the same value for Γ but slightly different values for the other polariton parameters in agreement with Yu's result.[6]

Finally, we show three figures, 14—16, of the external scattering cross section for all possible scattering channels ($1\rightarrow1'$, $1\rightarrow2'$, $2\rightarrow1'$, and $2\rightarrow2'$, as shown in Fig. 1) of LA Stokes scattering for the three ABC's, respectively, but with fixed Γ (equal to 1.0 cm^{-1}) value. The most characteristic feature in these figures is that the efficiency of the channel $1\rightarrow1'$ is the biggest of all for ABC2 and ABC3 mainly due to the smallness of the group and energy velocities near ω_L. Qualitative profile variation of the efficiency curves for three scattering channels $1\rightarrow1'$, $1\rightarrow2'$, and $2\rightarrow1'$, when changing the ABC is rather small compared with that for $2\rightarrow2'$.

V. SUMMARY AND DISCUSSION

We have calculated numerically the observable external scattering cross section for RBS, taking the A exciton in semiconducting CdS as a concrete example with both LA deformation potential and TA piezoelectric coupling. We used a factorization approximation and formulated the internal scattering cross section quantum mechanically, in contrast to BZB's semiclassical unified method.[4] We calculated numerically each factor contained in the cross-section formula: exciton-polariton dispersion curves, scattered frequency, transmissivities, group and energy velocities, and exciton-strength function, separately. We then joined them to calculate the internal scattering cross section and finally the observable external cross section. Although a completely unified treatment would be superior in that the factorization approximation could be avoided, our treatment has enabled us to elucidate which factors are crucially important and which ones are not in determining the external scattering cross section.

We pointed out the existence of the solid angle correction factor $n_j^{-2}(\omega_S)$ in the external scattering cross section, Eq. (2.2), and showed in Fig. 9 its importance in evaluating the cross section. A quantum-mechanical formulation of the internal scattering cross section was performed by Ovander[10] and Burstein and co-workers[11,12] but they did not discuss the external cross section, which is actually observed experimentally. As seen in Fig. 9 the solid angle correction factor strongly suppresses the resonance effect of the scattering cross section for the $2\rightarrow2'$ scattering channel when $\omega_I \gtrsim \omega_0$ and changes the curve profile. The transmissivity from vacuum to medium was also calculated to show how it varies with the choice of ABC's (Fig. 5), and influences qualitatively the profile of the scattering cross-section curves (Fig. 9). Again we want to emphasize the necessity of calculating the external scattering cross section instead of the internal one for comparison with experimental data. The most prominent feature of the transmissivity curves is the qualitative difference of the profile of curves with different ABC's. According to detailed numerical analysis, values of the reflectivity are sensitive to the exciton damping constant Γ, but the curve profile is rather insensitive to the choice of ABC's. Therefore, if we have little information on the value of Γ, it is very difficult to determine the proper ABC and Γ simultaneously from reflectivity data.

Although we cannot derive a compact analytic formula for the group velocity compared with that for the energy velocity, Eq. (4.14), our numerical calculations of the two velocities for mode-2 polaritons (Fig. 7) indicated that there is very little difference between them for $\Gamma < \Gamma_c$. They are easily shown to have correct limiting behavior both well below ω_0 and well above ω_L. We also observed a very small variation of the exciton-strength function with frequency in Fig. 8. In contrast to the perturbation approach[32] it does not contribute to the resonance effect of the scattering efficiency at all. Instead, the group and energy velocities are attributed to the resonance effect.

Our results for the external RBS cross section shown in Figs. 10—16 yield a large amount of interesting information. First we want to point out the qualitative variation of the curve profile with the choice of various ABC's, which leads to the great advantage of using RBS experiments for experimentally determining the proper ABC. Another advantage is that one can determine almost all parameters of excitons and polaritons with good accuracy, as described in Sec. IV B. Figure 10 shows the correct limiting behavior well below ω_0 where every ABC must give the same value of the scattering cross section. The next three figures, 11—13, exhibit an abrupt change in the scattering cross-section curve profile for each ABC when the exciton damping constant Γ approaches the threshold value Γ_c. This fact was first pointed out by Yu,[6] who calculated the scattering efficiency for ABC1 and ABC3, for a few Γ values, and found too small a value for Γ_c. We also note that the resonance behavior below ω_0 for $\Gamma < \Gamma_c$ is quite different from that for $\Gamma \gtrsim \Gamma_c$. As noted before, the anomalous behavior near $\Gamma \sim \Gamma_c$ comes from the drastic change of the polariton dispersion curves near Γ_c and their crossing for $\Gamma \geq \Gamma_c$, which also causes the abrupt change of the transmissivity curve profile. Physically the existence of Γ_c tells us that excitons and photons behave as if there were no interaction between them when $\Gamma \gtrsim \Gamma_c$. Therefore, as Yu noted, a sharp peak at ω_0 for $\Gamma \gtrsim \Gamma_c$ indicates the manifestation of the usual exciton resonance effect without the polariton effect, and the second sharp peak just above ω_0 comes from the resonance of the scattered wave. Strictly speaking, therefore, we observe the polariton scattering effect, not the resonance effect, for $\Gamma < \Gamma_c$, while only for $\Gamma \gtrsim \Gamma_c$ can the exciton resonance

effect of light scattering be observed. In the case of the A exciton in CdS one has $\Gamma_c = 11.5\ \text{cm}^{-1}$ from (4.3) and much experimental evidence suggests $\Gamma \lesssim 1\ \text{cm}^{-1}$. Therefore, one can expect polariton effects for RBS experiments in this case. For Cu_2O, however, a few experimental results suggest $\Gamma \sim 20\ \text{cm}^{-1}$, while $\Gamma_c \sim 1\ \text{cm}^{-1}$. In this case one cannot have any polariton effects except for some small bending behavior for the scattered frequency shifts. Interestingly, curves with $\Gamma = 10\ \text{cm}^{-1}$ in Figs. 10–12 have strong resemblance for all three ABC's to those obtained by BZB,[4] who took the same Γ value but slightly different values for other parameters, although their theoretical construction is quite different from ours. This implies a close connection between the two theories despite the apparent difference.

The last three figures, 14–16, indicate that the most appropriate scattering channel to investigate in order to choose the proper ABC for RBS experiments is $2 \rightarrow 2'$, since profile variation of the other three channels $1 \rightarrow 1'$, $1 \rightarrow 2'$, and $2 \rightarrow 1'$ are rather insensitive to the change of ABC's. The scattering cross section for the $1 \rightarrow 1'$ scattering channel has a maximum near ω_L for all ABC's due to the fact that the group and energy velocities become very small near ω_L for mode-1 polaritons.

It should be noted that a problem exists even when calculating the transmissivity from a *nonspatially* dispersive absorbing medium ($\Gamma \neq 0$) to vacuum. The incident and reflected electromagnetic waves in the medium can interfere constructively due to the absorption which results in an additional term in the transmissivity expression[33]

$$T = 1 - R + \frac{4\kappa^2/n}{(n+1)^2+\kappa^2}\ , \tag{5.1}$$

where R is the reflectivity from medium to vacuum which is given by

$$R = \frac{(n-1)^2+\kappa^2}{(n+1)^2+\kappa^2}\ , \tag{5.2}$$

n and κ are the real and imaginary parts of the refractive index in the medium. A consequence of Eq. (5.1) is that $T+R$ is greater than 1 for an absorbing medium. It should be noted, however, that the Poynting flux across the absorbing medium-vacuum boundary is continuous.

For spatially dispersive media, the same problem arises when one calculates the transmissivity. Detailed numerical analysis with ABC1 and ABC2 give as the sum of the two transmissivities, from vacuum to medium plus the reflectivity, the result

$$T_1(\omega) + T_2(\omega) + R(\omega) = 1.0$$

for all frequencies when $\Gamma = 0$. But when Γ is increased, ABC1 gives a sum greater than 1.0, ABC2 gives first a sum less than 1.0 around the frequency range of ω_0–ω_L, and finally both yield a sum much greater than 1.0 near ω_0 when $\Gamma \gtrsim \Gamma_c$. ABC3 does not yield the correct sum of 1.0 between ω_0 and ω_L even when $\Gamma = 0$, since it does not satisfy the energy-conservation requirement at the surface.[8] The same strange behavior is found near ω_0 for $\Gamma \gtrsim \Gamma_c$ as with ABC1 and ABC2. Actually, numerical calculations of the transmissivity of mode-2 polaritons exhibit a sharp peak near ω_0 for $\Gamma \gtrsim \Gamma_c$, the height of which increases unphysically beyond 1.0. This shortcoming may also be included implicitly in the BZB treatment, since, as described above, our results of the RBS efficiency for $\Gamma \sim \Gamma_c$ are very similar to theirs. The breakdown of the group velocity concept around the frequency range of ω_0–ω_L when $\Gamma > \Gamma_c$ also limits the validity of our treatment. Therefore, we believe that our approach is valid when $\Gamma < \Gamma_c$, except for the range of ω_0–ω_L when $\Gamma \gtrsim \Gamma_c$.

As is easily seen from the discussion in Sec. IV C it is straightforward to incorporate other ABC's (Ref. 34) into the scattering cross-section calculations. A slightly complicated but still straightforward extention of our theory is to incorporate the dead-layer effect into the calculation.[35] The calculation of the scattering cross section for magneto-RBS is also very interesting to compare with the experimental data to check the consistency of theory, especially, the choice of the proper ABC.

The last observation is the variation of the spectrum profile of the scattered wave, i.e., the profile variation of the differential scattering cross section Eq. (3.33), with the incident laser frequency ω_I as a parameter. Since factors such as the transmissivity as well as the well-known Lorentzian part contained in the cross section formula depend strongly on the scattered frequency, one may expect to have non-Lorentzian spectrum profiles. Even within the Lorentzian line profile approximation, the linewidth of the scattered wave given by Eq. (3.35) is strongly dependent on the incident laser frequency ω_I and is a maximum when $\omega_I \sim \omega_0$ for $2 \rightarrow 2'$ scattering as is easily seen from the imaginary part of the dispersion curves in Fig. 4. This implies two important points: First, experimental peak areas, instead of the heights, of RBS scattered light spectra must be measured to compare the data with the theoretical scattering cross section (3.36). Second, to calculate a realistic RBS spectrum profile we should do the convolution calculation of the differential scattering cross section with the instrumental resolution function, since otherwise the peak height may decrease when increasing incident frequency ω_I to ω_0 due to the small linewidths well below ω_0. By comparing the convoluted spectra with observed ones, one can determine the exciton damping constant Γ.

ACKNOWLEDGMENTS

The authors would like to thank J. L. Birman, M. Copic, C. Weisbuch, and W. Brenig for stimulating discussions. One of us (M.M.) is grateful to the members of the Computer Center at the City College of New York for their assistance. This research was supported by the National Science Foundation under Grant No. DMR-80-20835.

APPENDIX A: POLARITON-PHONON-INTERACTION HAMILTONIAN

Based on the idea of exciton-polaritons by Hopfield[2] and the exciton-phonon-interaction Hamiltonian, we will derive in this appendix the polariton-phonon-interaction Hamiltonian. It is one of the most basic ingredients in our discussion of RBS (or RRS). Let us assume that the

excitons under consideration have very weak interactions with phonons, impurities, etc. In other words, we assume that the exciton-phonon interaction can be treated perturbation theoretically. However, excitons couple bilinearly with photons via their polarization, bringing about composite particles called exciton polaritons.

First, we will derive the noninteracting polariton Hamiltonian from the exciton-photon coupled Hamiltonian;[2,16]

$$\mathscr{H}=\mathscr{H}_0+\mathscr{H}_{ER} , \tag{A1}$$

$$\mathscr{H}_0=\mathscr{H}_R+\mathscr{H}_E , \tag{A2}$$

$$\mathscr{H}_R=\sum_{\vec{k}}\hbar\tilde{c}k(a^{\dagger}_{\vec{k}}a_{\vec{k}}+\tfrac{1}{2}) , \tag{A3a}$$

$$\mathscr{H}_E=\sum_{\vec{k}}\hbar\omega_E(\vec{k})(b^{\dagger}_{\vec{k}}b_{\vec{k}}+\tfrac{1}{2}) , \tag{A3b}$$

$$\mathscr{H}_{ER}=\sum_{\vec{k}}\left[\hbar\left[\frac{4\pi\alpha_0\omega_0^2}{\epsilon_b}\right]^{1/2}\left[\frac{\omega_E(\vec{k})}{4\tilde{c}k}\right]^{1/2}\gamma_{\vec{k}}\psi^{\dagger}_{\vec{k}} + \frac{\pi\alpha_0\omega_0^2}{\epsilon_b}\frac{\hbar}{\tilde{c}k}\psi^{\dagger}_{\vec{k}}\psi_{\vec{k}}\right] , \tag{A4}$$

$$\psi_{\vec{k}}=a_{\vec{k}}+a^{\dagger}_{-\vec{k}} , \quad \gamma_{\vec{k}}=i(b_{\vec{k}}-b^{\dagger}_{-\vec{k}}) , \tag{A5}$$

where $a^{\dagger}_{\vec{k}},a_{\vec{k}}$ and $b^{\dagger}_{\vec{k}},b_{\vec{k}}$ are creation and annihilation operators of photons and excitons, respectively, $\tilde{c}=c/(\epsilon_b)^{1/2}$, $\omega_E(\vec{k})$ is the exciton frequency $[\omega_0=\omega_E(k=0)]$, α_0 the exciton polarizability, and ϵ_b the background dielectric constant. Since the interaction between photons and excitons, $\mathscr{H}_{ER}$, is bilinear, one can diagonalize $\mathscr{H}$ by a canonical transformation to obtain the noninteracting exciton-polariton Hamiltonian. In the following we put $\hbar=1$ for convenience. Let us define a linear combination

$$\alpha_{\vec{k}}=wa_{\vec{k}}+xb_{\vec{k}}+ya^{\dagger}_{-\vec{k}}+zb^{\dagger}_{-\vec{k}} . \tag{A6}$$

If $\alpha_{\vec{k}}$ is to be a normal-mode annihilation operator for $\mathscr{H}$, it must satisfy the following equation:

$$[\alpha_{\vec{k}},\mathscr{H}]=\omega\alpha_{\vec{k}} , \tag{A7}$$

where ω is the normal-mode eigenfrequency. Substituting (A6) and (A1) into (A7) and using the boson commutation relations for a and b, we obtain four homogeneous equations for w, x, y, and z and derive the following secular equation:

$$\begin{vmatrix} \tilde{c}k+2D-\omega & -iC & -2D & -iC \\ -iC & \omega_E-\omega & -iC & 0 \\ 2D & -iC & -(\tilde{c}k+2D+\omega) & -iC \\ -iC & 0 & iC & -(\omega_E+\omega) \end{vmatrix}=0 ,$$

where we set

$$C\equiv[4\pi\alpha_0\omega_0^2\omega_E(\vec{k})/4\epsilon_b\tilde{c}k]^{1/2} , \quad D\equiv\pi\alpha_0\omega_0^2/\epsilon_b\tilde{c}k .$$

The secular equation is straightforwardly solved to give the following simple result:

$$\left[\frac{\tilde{c}k}{\omega}\right]^2=1+\frac{4\pi\alpha_0\omega_0^2/\epsilon_b}{\omega_E^2(\vec{k})-\omega^2} . \tag{A8}$$

This is exactly the exciton-polariton dispersion equation, (3.6), with $\Gamma=0$.

The dispersion equation, (A8), has two independent solutions (or two normal modes or branches), $\omega_1(\vec{k})$ and $\omega_2(\vec{k})$, for a given wave vector $\vec{k}$. Therefore, there are two independent polariton annihilation operators, $\alpha_{\vec{k}1}$ and $\alpha_{\vec{k}2}$, which satisfy the usual boson commutation relations

$$[\alpha_{\vec{k}i},\alpha_{\vec{k}'j}]=[\alpha^{\dagger}_{\vec{k}i},\alpha^{\dagger}_{\vec{k}'j}]=0 ,$$
$$[\alpha_{\vec{k}i},\alpha^{\dagger}_{\vec{k}'j}]=\delta_{ij}\delta_{\vec{k}\vec{k}'} . \tag{A9}$$

Now the noninteracting exciton-polariton Hamiltonian takes a simple form,

$$\mathscr{H}_P=\sum_{\vec{k}}\sum_{i=1}^{2}\omega_i(\vec{k})(\alpha^{\dagger}_{\vec{k}i}\alpha_{\vec{k}i}+\tfrac{1}{2}) . \tag{A10}$$

The transformation matrix (C_{ij}) is defined by

$$\begin{pmatrix} \alpha_{\vec{k}1} \\ \alpha_{\vec{k}2} \\ \alpha^{\dagger}_{-\vec{k}1} \\ \alpha^{\dagger}_{-\vec{k}2} \end{pmatrix}=\underline{C}\begin{pmatrix} a_{\vec{k}} \\ b_{\vec{k}} \\ a^{\dagger}_{-\vec{k}} \\ b^{\dagger}_{-\vec{k}} \end{pmatrix} . \tag{A11}$$

Relations among C_{ij}'s are derived from, e.g.,

$$\alpha^{\dagger}_{-\vec{k}1}=(\alpha_{-\vec{k}1})^{\dagger} , \quad C_{31}(\vec{k})=C^*_{13}(-\vec{k}) ,$$
$$C_{32}(\vec{k})=C^*_{14}(-\vec{k}) , \quad C_{33}(\vec{k})=C^*_{11}(-\vec{k}) ,$$
$$C_{34}(\vec{k})=C^*_{12}(-\vec{k}) , \quad C_{41}(\vec{k})=C^*_{23}(-\vec{k}) ,$$
$$C_{42}(\vec{k})=C^*_{24}(-\vec{k}) , \quad C_{43}(\vec{k})=C^*_{21}(-\vec{k}) ,$$
$$C_{44}(\vec{k})=C^*_{22}(-\vec{k}) .$$

Elements of the inverse transformation $(C^{-1})_{ij}$, defined by

$$\begin{pmatrix} a_{\vec{k}} \\ b_{\vec{k}} \\ a^{\dagger}_{-\vec{k}} \\ b^{\dagger}_{-\vec{k}} \end{pmatrix}=\underline{C}^{-1}\begin{pmatrix} \alpha_{\vec{k}1} \\ \alpha_{\vec{k}2} \\ \alpha^{\dagger}_{-\vec{k}1} \\ \alpha^{\dagger}_{-\vec{k}2} \end{pmatrix} , \tag{A12}$$

are expressed with C_{ij} by taking commutators such as $[a_{\vec{k}},\alpha^{\dagger}_{\vec{k}1}]$ and substituting (A11) on the one hand, and (A12) on the other hand, with the help of the commutation relations both for a and b, and for α_1 and α_2;

$$C^{-1}=\begin{pmatrix} C^*_{11} & C^*_{21} & -C^*_{31} & -C^*_{41} \\ C^*_{12} & C^*_{22} & -C^*_{32} & -C^*_{42} \\ -C^*_{13} & -C^*_{23} & C^*_{33} & C^*_{43} \\ -C^*_{14} & -C^*_{24} & C^*_{34} & C^*_{44} \end{pmatrix} . \tag{A13}$$

In order to obtain concrete expressions for the different components of the C_{ij}'s, additional relations are needed to supplement the secular equations derived from (A7). Let us pay attention to the fact that polariton energy density can be expressed in terms of the C_{ij}'s.

The average polariton energy is written as a sum of the averaged electromagnetic and mechanical (exciton) energies;[16,27] $\overline{W}_t=\overline{W}_{EM}+\overline{W}_{ex}$. This expression is easily shown to take the form

$$\overline{W}_t=\frac{\epsilon_b\omega_E^4}{8\pi(\omega_E^2-\omega^2)}\left[\left[1-\frac{\omega^2}{\omega_E^2}\right]^2+\frac{4\pi\alpha_0\omega_0^2}{\epsilon_b\omega_E^2}\right]\langle\,|E|^2\rangle\,, \tag{A14}$$

in terms of $\langle\,|E|^2\rangle$ [or, if necessary, in terms of $\langle\,|P_{ex}|^2\rangle$ via the relation $\vec{P}_{ex}=\alpha_0\omega_0^2/(\omega_E^2-\omega^2)\vec{E}$]. The electric and polarization fields are expressed in terms of annihilation and creation operators of photons and polarization wave quanta (i.e., excitons) as follows[2] ($\hbar=1$):

$$\vec{E}(\vec{r})=\sum_{\vec{k}\lambda} i\left[\frac{2\pi\tilde{c}k}{\epsilon_b V}\right]^{1/2}\hat{e}(\vec{k},\lambda)(a_{\vec{k}\lambda}-a^{\dagger}_{-\vec{k}\lambda})e^{i\vec{k}\cdot\vec{r}}\,, \tag{A15a}$$

$$\vec{P}_{ex}(\vec{r})=\sum_{\vec{k}\lambda}\left[\frac{\omega_E\alpha_0}{2V}\right]^{1/2}\hat{e}(\vec{k},\lambda)(b_{\vec{k}\lambda}+b^{\dagger}_{-\vec{k}\lambda})e^{i\vec{k}\cdot\vec{r}}\,. \tag{A15b}$$

The average values of the absolute square of the fields with wave vector $\vec{k}$ are (for unit volume V),

$$\langle\,|E_{\vec{k}}|^2\rangle=\frac{4\pi\tilde{c}k}{\epsilon_b}\langle\,|a_{\vec{k}}-a^{\dagger}_{-\vec{k}}|^2\rangle\,, \tag{A16a}$$

$$\langle\,|P_{ex,\vec{k}}|^2\rangle=\omega_E\alpha_0\langle\,|b_{\vec{k}}+b_{-\vec{k}}|^2\rangle\,. \tag{A16b}$$

The substitution of Eq. (A12) and (A16a) into (A14) yields with the use of (A13)

$$\overline{W}_{t\vec{k}}=\sum_{i=1,2}\frac{\tilde{c}k\omega_E^4}{(\omega_E^2-\omega_i^2)^2}\left[\left[1-\frac{\omega_i^2}{\omega_E^2}\right]^2+\frac{4\pi\alpha_0\omega_0^2}{\epsilon_b\omega_E^2}\right]\times|C_{i1}+C_{i3}|^2(n_{\vec{k}i}+\tfrac{1}{2})\,, \tag{A17}$$

where $n_{\vec{k}i}=\langle\alpha^{\dagger}_{\vec{k}i}\alpha_{\vec{k}i}\rangle$ ($i=1,2$) and ω_i is the mode-i exciton-polariton frequency.

On the other hand, the energy density of the exciton polariton is also expressed from (A10) as ($\hbar=V=1$)

$$\overline{W}_{t\vec{k}}=\sum_{i=1,2}\omega_i(n_{\vec{k}i}+\tfrac{1}{2})\,. \tag{A18}$$

Equating (A18) with (A17) and taking mode-2 polaritons as an example, we have the relation

$$|C_{21}+C_{23}|^2=\frac{\omega_2(\omega_E^2-\omega_2^2)^2}{\tilde{c}k\omega_E^4}\left[\left[1-\frac{\omega_2^2}{\omega_E^2}\right]^2+\frac{4\pi\alpha_0\omega_0^2}{\epsilon_b\omega_E^2}\right]^{-1} \tag{A19}$$

This is the required additional relation for C_{2j} ($j=1$–4). Equation (A19) and the four homogeneous equations for C_{2j} derived from (A7) can be solved straightforwardly to give

$$C_{21}=\left[1-\frac{\omega_2^2}{\omega_E^2}\right]\left[\frac{\tilde{c}k}{\omega_E}+\frac{\omega_2}{\omega_E}\right]\Big/2\left\{\left[\frac{\tilde{c}k\omega_2}{\omega_E^2}\right]\left[\left[1-\frac{\omega_2^2}{\omega_E^2}\right]^2+\frac{4\pi\alpha_0\omega_0^2}{\epsilon_b\omega_E^2}\right]\right\}^{1/2},$$

$$C_{22}=-i\left[\frac{\pi\alpha_0\omega_0^2}{\epsilon_b\omega_E^2}\right]^{1/2}\left[1+\frac{\omega_2}{\omega_E}\right]\Big/\left\{\left[\frac{\omega_2}{\omega_E}\right]\left[\left[1-\frac{\omega_2^2}{\omega_E^2}\right]^2+\frac{4\pi\alpha_0\omega_0^2}{\epsilon_b\omega_E^2}\right]\right\}^{1/2}, \tag{A20}$$

$$C_{23}=\frac{\omega_2-\tilde{c}k}{\omega_2+\tilde{c}k}C_{21}\,,$$

$$C_{24}=\frac{\omega_E-\omega_2}{\omega_E+\omega_2}C_{22}\,.$$

Precisely speaking there still remains a small ambiguity about the sign ($\pm$) in deriving (A20). We have used the convention that in the limit of $\vec{k}\to\vec{0}$ and $\alpha_0\to 0$ (no interactions between photons and excitons) one has $\alpha_{\vec{k}1}=b_{\vec{k}}$, $\alpha^{\dagger}_{-\vec{k}1}=b^{\dagger}_{-\vec{k}}$ (excitons); $\alpha_{\vec{k}2}=a_{\vec{k}}$, $\alpha^{\dagger}_{-\vec{k}2}=a^{\dagger}_{-\vec{k}}$ (photons). In (A20) we cited only the C_{2j}'s which are associated with the mode-2 polaritons. Other C_{ij}'s can be obtained from (A20) by replacing ω_2 by ω_i with $\omega_3=-\omega_1$, $\omega_4=-\omega_2$, and multiplying by i (imaginary unit number) for $i=1,3$ and by -1 for $i=4$.

As yet we have completely neglected interactions between excitons and other excitations such as phonons, since in polar crystals the exciton-photon interaction is the strongest. In order to discuss light scattering in polar crystals, however, one must derive a polariton-phonon-interaction Hamiltonian. The polariton-phonon interaction is known to arise mainly from the exciton-phonon interaction

$$\mathscr{H}_{EL}=iV^{-1/2}\sum_{\vec{q},\vec{k}}\Gamma_0(\vec{q})b^{\dagger}_{\vec{k}+\vec{q}}b_{\vec{k}}(c_{\vec{q}}-c^{\dagger}_{-\vec{q}})\,, \tag{A21}$$

where $\Gamma_0(\vec{q})$ denotes the exciton-phonon-interaction kernel and $c_{\vec{q}}$ is the phonon annihilation operator. Transforming the exciton operators to polariton operators via Eq. (A12), we have the polariton-phonon-interaction Hamiltonian

$$\mathscr{H}_{PL}=iV^{-1/2}\sum_{\vec{q},\vec{k}}\Gamma_0(\vec{q})\sum_{j,l}(\underline{C}^{-1}_{\vec{k}+\vec{q}})_{4j}(\underline{C}^{-1}_{\vec{k}})_{2l}\alpha_{-\vec{k}-\vec{q},j}\alpha_{\vec{k},l}(c_{\vec{q}}-c^{\dagger}_{-\vec{q}}),$$

where we have used the notations $\alpha_{\vec{k}3}=\alpha^{\dagger}_{-\vec{k}1}$ and $\alpha_{\vec{k}4}=\alpha^{\dagger}_{-\vec{k}2}$. Let us pay attention to mode-i to -j polariton scattering by phonons. Then there are two terms for experimentally accessible interactions: $\alpha^{\dagger}_{\vec{k}+\vec{q},j}\alpha_{\vec{k},i}(c_{\vec{q}}-c^{\dagger}_{-\vec{q}})$ and $\alpha_{-\vec{k}-\vec{q},i}\alpha^{\dagger}_{-\vec{k},j}(c_{\vec{q}}-c^{\dagger}_{-\vec{q}})$. The polariton-phonon-interaction Hamiltonian associated with light scattering by one phonon can then be written for the mode-i to -j scattering as

$$\mathscr{H}^{ij}_{PL}=(i)^{j-i+1}V^{-1/2}\sum_{\vec{q},\vec{k}}\Gamma_0(\vec{q})A_{ij}(\vec{k},\vec{k}+\vec{q})\alpha^{\dagger}_{\vec{k}+\vec{q},j}\alpha_{\vec{k},i}(c_{\vec{q}}-c_{-\vec{q}}), \tag{A22}$$

where superscripts i and j of the imaginary number unit i denote the polariton mode (1 or 2) and

$$A_{ij}(\vec{k},\vec{k}+\vec{q})=\tfrac{1}{2}A_i^{1/2}(\vec{k})\left[1+\frac{\omega_E(\vec{k})\omega_E(\vec{k}+\vec{q})}{\omega_i(\vec{k})\omega_j(\vec{k}+\vec{q})}\right]\times A_j^{1/2}(\vec{k}+\vec{q}), \tag{A23a}$$

$$A_i(\vec{k})=\frac{4\pi\alpha_0\omega_0^2\omega_E(\vec{k})\omega_i(\vec{k})}{[\omega_E^2(\vec{k})-\omega_i^2(\vec{k})]^2}\Big/\left[\epsilon_b+\frac{4\pi\alpha_0\omega_0^2\omega_E^2(\vec{k})}{[\omega_E^2(\vec{k})-\omega_i^2(\vec{k})]^2}\right]. \tag{A23b}$$

The quantity $A_i(\vec{k})$ is the exciton-strength function discussed in Sec. IV E. The result (A22) is equivalent to that derived by Burstein *et al.*[11] For convenience we rewrite it as follows:

$$\mathscr{H}^{ij}_{PL}=(i)^{j-i}V^{-1/2}\sum_{\vec{k},\vec{k}',\vec{q}}\Gamma_0(\vec{q})A_{ij}(\vec{k},\vec{k}')\times\delta_{\vec{k}',\vec{k}+\vec{q}}\alpha^{\dagger}_{\vec{k}',j}\alpha_{\vec{k},i}\varphi_{\vec{q}}, \tag{A24}$$

where we set

$$\varphi_{\vec{q}}=i(c_{\vec{q}}-c_{-\vec{q}}). \tag{A25}$$

APPENDIX B: THRESHOLD VALUE OF THE EXCITON DAMPING CONSTANT Γ_c

First, we rewrite the exciton-polariton dispersion equation (3.6) in a more convenient form by replacing ω, ω_0, and Γ by $2\pi c\bar{\omega}$, $2\pi c\bar{\omega}_0$, and $2\pi c\bar{\Gamma}$, respectively, and k by $2\pi\bar{k}$. Then, by removing the bars, one obtains

$$\frac{k^2}{\omega^2}=\epsilon_b+\frac{A\omega_0^2}{Bk^2+\Delta\Omega^2}, \tag{B1}$$

where $A=4\pi\alpha_0$, $B=2\pi\hbar\omega_0/m^*c$, and $\Delta\Omega^2=\omega_0^2-\omega^2-i\omega\Gamma$. Now ω, ω_0, k, and Γ are in units of wave numbers (cm^{-1}). Note that ω_0 in the definition of B in the text is in units of sec^{-1}.

As stressed earlier our experimental situation (RBS experiment) imposes the condition of real ω, and complex k (forced harmonic-oscillator model). Then Eq. (B1) is regarded as a simple biquadratic equation for k and the two solutions k_1 and k_2 for a given ω are given formally by

$$C_1=\epsilon_b B\omega^2-\Delta\Omega^2,\quad C_2=\epsilon_b\omega^2\Delta\Omega^2+A\omega_0^2\omega^2,$$
$$C_3=C_1^2+4BC_2,\quad C_4=(C_3)^{1/2},\quad C_5=C_1-C_4,$$
$$C_6=C_1+C_4,\quad k_1=(C_5/2B)^{1/2},\quad k_2=(C_6/2B)^{1/2}. \tag{B2}$$

Since the complex square root is involved in the solutions (B2), we first use the argument convention $(-\pi, +\pi)$ on the complex plane.

Next let us persue the movement of C_3 on the complex plane as a function of ω with various Γ values. C_3 is written explicitly as

$$C_3(\omega)=\{(1-\epsilon_b B)^2\omega^4-[2(1-\epsilon_b B-2AB)\omega_0^2+\Gamma^2]\omega^2+\omega_0^4\}+2i\omega\Gamma[(1-\epsilon_b B)\omega^2-\omega_0^2]. \tag{B3}$$

$\mathrm{Re}C_3(\omega)$ has extrema at $\omega=0$ and ω_t, where ω_t is given by

$$\omega_t^2=\frac{2(1-\epsilon_b B-2AB)\omega_0^2+\Gamma^2}{2(1-\epsilon_b B)^2}\approx\omega_0^2. \tag{B4}$$

In other words, the tangent line at the points $C_3(0)$ and $C_3(\omega_t)$ is parallel to the $\mathrm{Im}C_3$ axis. ω_t is extremely close to ω_0, since $\epsilon_b B\ll 1$, $AB\ll 1$, and $\Gamma\ll\omega_0$ (for the A exciton in CdS, $\epsilon_b\sim 9.3$, $B\sim 5.6\times10^{-6}$, $A\sim 1.4\times10^{-2}$, $\Gamma\sim 1$ cm^{-1}, and $\omega_0\sim 20\,590$ cm^{-1}). At ω_t we have

$$\mathrm{Re}C_3(\omega=\omega_t)=\omega_0^4-\frac{[2(1-\epsilon_b B-2AB)\omega_0^2+\Gamma^2]^2}{4(1-\epsilon_b B)^2}. \tag{B5}$$

On the other hand, $\mathrm{Im}C_3=0$ at $\omega=\tilde{\omega}_0$, where

$$\tilde{\omega}_0=\omega_0/(1-\epsilon_b B)^{1/2}\approx\omega_0. \tag{B6}$$

Again, $\tilde{\omega}_0$ is very close to ω_0. Therefore, the curve of $C_3(\omega)$ on the complex plane passes over the $\mathrm{Re}C_3$ axis at $\omega=\tilde{\omega}_0\approx\omega_t\approx\omega_0$, where the tangent line is almost parallel with the $\mathrm{Im}C_3$ axis. The value of $\mathrm{Re}C_3$ is given by

$$\mathrm{Re}C_3(\omega=\tilde{\omega}_0)=\frac{(4AB\omega_0^2-\Gamma)\omega_0^2}{1-\epsilon_b B}. \tag{B7}$$

Therefore, when Γ equals Γ_c, which is defined as

$$\Gamma_c=(4AB\omega_0^2)^{1/2}, \tag{B8}$$

the C_3 curve crosses the origin, in which case $\tilde{\omega}_0$ is exactly equal to ω_t. For $\Gamma<\Gamma_c$ ($\Gamma>\Gamma_c$), $\mathrm{Re}C_3(\omega=\tilde{\omega}_0)>0$ (<0). In other words, when $\Gamma>\Gamma_c$, the C_3 curve moves around the origin. Figure 17 shows schematically the results dis-

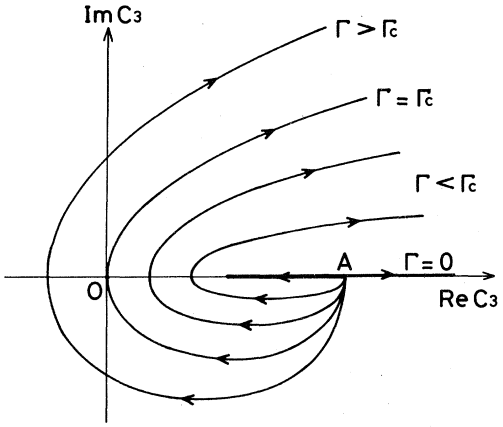

FIG. 17. Schematic representation of the movement (illustrated by arrows) of C_3 on the complex plane when varying both ω (from 0 to ∞), and Γ. C_3 starts from the point A. For $\Gamma < \Gamma_c$ the C_3 curves pass over the positive part of ReC_3 axis. However, for $\Gamma > \Gamma_c$ they cross the negative part of ReC_3 (move around the origin).

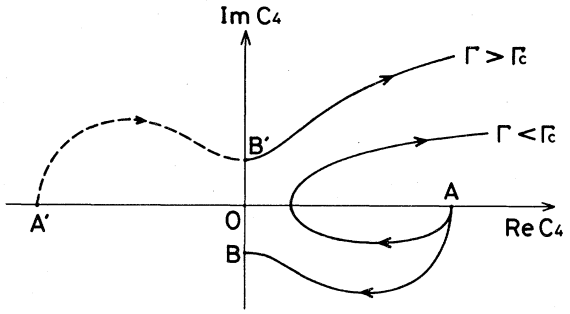

FIG. 18. Schematic representation of the movement of $C_4=(C_3)^{1/2}$ on the complex plane when varying both ω (from 0 to ∞) and Γ. For $\Gamma < \Gamma_c$, C_4 starts from point A and moves continuously under the original argument convention. However, for $\Gamma > \Gamma_c$ it exhibits an unphysical discontinuity from B to B'. In the latter case a new argument convention must be used to obtain a continuous $C_4(\omega)$ movement such as the one shown by the joint curve with dashed and solid lines. Now C_4 starts from the point A'.

cussed above.

Next, let us investigate the movement of $C_4=(C_3)^{1/2}$ on the complex plane in order to study the effect of Γ_c on the dispersion curves. We study two ranges of Γ.

(a) $\Gamma < \Gamma_c$: Starting from point A, $C_4(\omega)$ moves continuously when varying ω from 0 to infinity, as shown in Fig. 18.

(b) $\Gamma > \Gamma_c$: Owing to the argument convention defined before, when $C_3(\omega)$ crosses the negative part of ReC_3 axis, C_4 exhibits an unphysical discontinuity from the point B to B' at $\omega=\tilde{\omega}_0$ ($\approx\omega_0$) in the figure. To avoid this discontinuity we must choose another argument convention $(0,2\pi)$ for this case (or use the Reimann surface). We then obtain a continuous movement for the C_4 curve starting from the point A' (instead of A) when varying ω from 0 to infinity. This is shown in Fig. 18 by the joint curve consisting of dashed and solid lines.

Thus one must choose the proper argument convention according to the Γ value in order to avoid the unphysical discontinuity in the dispersion curves. Detailed numerical analysis shows that the imaginary part of both C_5 and C_6 is always positive. In other words, after obtaining a continuous C_4 one can obtain dispersion curves without changing the agrument convention. The dispersion curves thus obtained are shown in Fig. 4 in the text.

The physical consequence of the argument change for C_4 is very interesting. When $\Gamma < \Gamma_c$ we have the usual polariton dispersion curves. For example, the mode-2 (or outer, or lower branch) curve exhibits a photonlike behavior for $\omega < \omega_0$, then changes quickly and continuously to show an excitonlike behavior for $\omega > \omega_0$. When $\Gamma > \Gamma_c$, however, the photonlike curve for $\omega < \omega_0$ also exhibits a photonlike behavior for $\omega > \omega_L$ after crossing the excitonlike branch curve between ω_0 and ω_L. In other words, when $\Gamma > \Gamma_c$, excitons and photons behave as if there were no interaction between them.

---

*Present address: Research Institute of Electrical Communication, Tohoku University, Sendai 980, Japan.

†Present address: Physics Department, Brookhaven National Laboratory, Upton, NY 11973.

[1]S. I. Pekar, Zh. Eksp. Teor. Fiz. 33, 1022 (1957) [Sov. Phys.—JETP 6, 785 (1958)]; Fiz. Tverd. Tela Leningrad 4, 1301 (1962) [Sov. Phys.—Solid State 4, 953 (1962)].

[2]J. J. Hopfield, Phys. Rev. 112, 1555 (1958).

[3]J. J. Hopfield and D. G. Thomas, Phys. Rev. 132, 563 (1963).

[4]W. Brenig, R. Zeyher, and J. L. Birman, Phys. Rev. B 6, 4617 (1972).

[5]For the most recent discussion on this matter, see the review article by J. L. Birman, in *Excitons,* edited by E. I. Rashba and M. D. Sturge (North-Holland, Amsterdam, 1982).

[6]P. Y. Yu, Solid State Commun. 32, 29 (1979).

[7]For more detailed information see the review article by B. Bendow, *Polariton Theory of Resonance Raman Scattering in Solids,* Vol. 82 of *Springer Tracts in Modern Physics* (Springer, Berlin, 1978), p. 69.

[8]R. Zeyher, C. S. Ting, and J. L. Birman, Phys. Rev. B 10, 1725 (1974).

[9]D. R. Tilley, J. Phys. C 13, 781 (1980).

[10]L. N. Ovander, Fiz. Tverd. Tela Leningrad 3, 2394 (1961) [Sov. Phys.—Solid State 3, 1737 (1962)]; 4, 1471 (1962) [4, 1081 (1962)].

[11]E. Burstein, D. L. Mills, A. Pinczuk, and S. Ushioda, Phys. Rev. Lett. 22, 348 (1969); 22, 913(E) (1969).

[12]D. L. Mills and E. Burstein, Phys. Rev. 188, 1465 (1969).

[13]A. S. Barker, Jr. and R. Loudon, Rev. Mod. Phys. 44, 18 (1972).

[14]J. R. Sandercock, Phys. Rev. Lett. 29, 1735 (1972).

[15]A. Dervish and R. Loudon, J. Phys. C 9, L669 (1976).

[16]W. C. Tait, Phys. Rev. B 5, 648 (1972).

[17]D. N. Zubarev, Usp. Fiz. Nauk 71, 71 (1960) [Sov. Phys.—Usp. 3, 320 (1960)].

[18]R. Loudon, J. Phys. C 11, 403 (1978).

[19]J. J. Sein, Phys. Lett. 32A, 141 (1970); J. L. Birman and J. J. Sein, Phys. Rev. B 6, 2482 (1972).
[20]A. A. Maradudin and D. L. Mills, Phys. Rev. B 7, 2787 (1973).
[21]G. S. Agarwal, D. N. Pattanayak, and E. Wolf, Phys. Rev. Lett. 27, 1022 (1971); Phys. Rev. B 10, 1477 (1974).
[22]V. M. Agranovich and V. L. Ginzburg, *Spatial Dispersion in Crystal Optics and the Theory of Excitons* (Interscience, New York, 1966).
[23]M. J. Frankel and J. L. Birman, Phys. Rev. B 13, 2587 (1976).
[24]R. Zeyher, J. L. Birman, and W. Brenig, Phys. Rev. B 6, 4613 (1972).
[25]C. S. Ting, M. Frankel, and J. L. Birman, Solid State Commun. 17, 1285 (1975).
[26]See, e.g., L. D. Landau and E. M. Lifshitz, *Electrodynamics of Continuous Media* (Pergamon, New York, 1960).
[27]R. Loudon, J. Phys. A 3, 233 (1970).
[28]A. V. Sel'kin, Fiz. Tverd. Tela Leningrad 19, 2433 (1977) [Sov. Phys.—Solid State 19, 1424 (1977)].
[29]M. Nakayama, Solid State Commun. 45, 821 (1983).
[30]D. L. Mills and E. Burstein, Rep. Prog. Phys. 37, 817 (1974).
[31]P. Y. Yu, in *Light Scattering in Solids,* edited by J. L. Birman, H. Z. Cummins, and K. K. Rebane (Plenum, New York, 1979), p. 143.
[32]J. L. Birman and A. K. Ganguly, Phys. Rev. Lett. 17, 647 (1966); A. K. Ganguly and J. L. Birman, Phys. Rev. 162, 806 (1967).
[33]K. H. Beckmann and B. Casper, Philips Res. Rep. 20, 190 (1965).
[34]M. F. Bishop and A. A. Maradudin, Phys. Rev. B 14, 3384 (1976).
[35]P. Y. Yu and F. Evangelisti, Phys. Rev. Lett. 42, 1642 (1979).